



UNIVERSITY OF LEEDS

This is a repository copy of *Recent unrest (2002–2015) imaged by space geodesy at the highest risk Chilean volcanoes: Villarrica, Llaima, and Calbuco (Southern Andes)*.

White Rose Research Online URL for this paper:
<http://eprints.whiterose.ac.uk/116790/>

Version: Accepted Version

Article:

Delgado, F, Pritchard, ME, Ebmeier, S orcid.org/0000-0002-5454-2652 et al. (2 more authors) (2017) *Recent unrest (2002–2015) imaged by space geodesy at the highest risk Chilean volcanoes: Villarrica, Llaima, and Calbuco (Southern Andes)*. *Journal of Volcanology and Geothermal Research*, 344. pp. 270-288. ISSN 0377-0273

<https://doi.org/10.1016/j.jvolgeores.2017.05.020>

© 2017 Elsevier B.V. This manuscript version is made available under the CC-BY-NC-ND 4.0 license <http://creativecommons.org/licenses/by-nc-nd/4.0/>

Reuse

Items deposited in White Rose Research Online are protected by copyright, with all rights reserved unless indicated otherwise. They may be downloaded and/or printed for private study, or other acts as permitted by national copyright laws. The publisher or other rights holders may allow further reproduction and re-use of the full text version. This is indicated by the licence information on the White Rose Research Online record for the item.

Takedown

If you consider content in White Rose Research Online to be in breach of UK law, please notify us by emailing eprints@whiterose.ac.uk including the URL of the record and the reason for the withdrawal request.

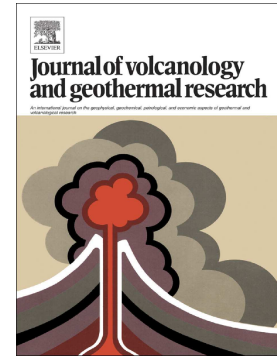


eprints@whiterose.ac.uk
<https://eprints.whiterose.ac.uk/>

Accepted Manuscript

Recent unrest (2002–2015) imaged by space geodesy at the highest risk Chilean volcanoes: Villarrica, Llaima, and Calbuco (Southern Andes)

Francisco Delgado, Matthew E. Pritchard, Susanna Ebmeier, Pablo González, Luis Lara



PII: S0377-0273(17)30308-6
DOI: doi: [10.1016/j.jvolgeores.2017.05.020](https://doi.org/10.1016/j.jvolgeores.2017.05.020)
Reference: VOLGEO 6105

To appear in: *Journal of Volcanology and Geothermal Research*

Received date: 18 May 2016
Revised date: 2 May 2017
Accepted date: 19 May 2017

Please cite this article as: Francisco Delgado, Matthew E. Pritchard, Susanna Ebmeier, Pablo González, Luis Lara , Recent unrest (2002–2015) imaged by space geodesy at the highest risk Chilean volcanoes: Villarrica, Llaima, and Calbuco (Southern Andes), *Journal of Volcanology and Geothermal Research* (2017), doi: [10.1016/j.jvolgeores.2017.05.020](https://doi.org/10.1016/j.jvolgeores.2017.05.020)

This is a PDF file of an unedited manuscript that has been accepted for publication. As a service to our customers we are providing this early version of the manuscript. The manuscript will undergo copyediting, typesetting, and review of the resulting proof before it is published in its final form. Please note that during the production process errors may be discovered which could affect the content, and all legal disclaimers that apply to the journal pertain.

Recent unrest (2002-2015) imaged by space geodesy at the highest risk Chilean volcanoes: Villarrica, Llaima, and Calbuco (Southern Andes)

Francisco Delgado ⁽¹⁾, Matthew E. Pritchard ⁽¹⁾, Susanna Ebmeier⁽²⁾, Pablo González⁽³⁾, Luis Lara ⁽⁴⁾

⁽¹⁾ Department of Earth and Atmospheric Sciences, Cornell University, Ithaca, NY, 14853, USA. ⁽²⁾ School of Earth and Environment, University of Leeds, Leeds, UK. ⁽³⁾ School of Environmental Sciences, University of Liverpool, Liverpool, UK. ⁽⁴⁾ Servicio Nacional de Geología y Minería, Chile.

Corresponding author: fjd49@cornell.edu

Villarrica, Llaima, and Calbuco volcanoes are the most active and dangerous volcanoes in the Southern Andes, and we use Interferometric Synthetic Aperture Radar (InSAR) observations from multiple satellites (ERS-2, ENVISAT, ALOS, RADARSAT-2, COSMO-SkyMed, TerraSAR-X, Sentinel-1A and ALOS-2) to constrain ground deformation that spans episodes of unrest and eruption at all three volcanoes between 2002 and 2015. We find episodes of ground deformation at each volcano, which we invert using analytic elastic half space models to make some of the first geophysical inferences about the source depths of potential magma chambers. At Llaima, we interpret that the VEI 2 April 3 2009 eruption was preceded by ~6-15 cm of precursory ground uplift one month before from a source ~5 km below the surface on the western side of the edifice. The VEI 2 March 3 2015 Villarrica eruption was followed by a short lived uplift of 5 cm in the SE part of the volcano from a source depth of ~6 km. The VEI 4 April 22-23 2015 Calbuco eruption produced 12 cm of coeruptive subsidence from a source depth 8-11 km and offset ~2 km S from the summit. Importantly, we do not find clear evidence that the January 1 2008, the March 3 2015 and April 22 2015 eruptions at Llaima, Villarrica and Calbuco volcanoes were preceded by either transient or continuous ground uplift. There are several possible explanations for the lack of precursory deformation at each volcano – it is possible that any precursory deformation occurred only hours before

the eruption (e.g., at Calbuco), pre-eruptive inflation was canceled by co-eruptive subsidence (as we inferred happened during the April 2009 Llaima eruption), the pre-eruptive deformation was too small to be detectable in areas with persistent topography correlated phase delays, pressurized source are deep, or that open-vent volcanoes like Villarrica and Llaima do not pressurize. At all three volcanoes, X and C band interferograms decorrelate in a few weeks due to vegetation, snow and ice, and have persistent atmospheric phase delays that we find cannot be reliably removed with available global weather models. The low number of SAR acquisitions therefore makes it challenging to reliably measure unaliased deformation. We recommend a multi-satellite observing strategy with short repeat periods, frequently acquired high-resolution digital elevation models, and with acquisitions during every satellite overflight that may improve the temporal resolution of measurements.

Keywords: InSAR, volcano geodesy, southern Andes, Llaima, Villarrica, Calbuco.

1. Introduction

Ground deformation measured by space geodetic techniques such as InSAR is one of the most used data sets to constrain the rates of magma transport and storage in active volcanoes and the geometry and location of the plumbing systems that produce eruptions (e.g., Dvorak and Dzurisin (1997); Dzurisin (2003); Dzurisin and Lu (2006); Pinel et al. (2014); Acocella et al. (2015)). However, not all the eruptions are related to ground deformation and hence this relationship, unique to each volcano, is not always straightforward (e.g., Biggs et al. (2014); Acocella et al. (2015)). To understand the relation between deformation and eruptions for each volcano, we need dense temporal and spatial observations of ground deformation over several eruptions as well as periods of quiescence and unrest. Ground deformation should also be related to degassing and seismicity measurements, to provide more robust constraints on magma dynamics (Anderson and Poland, 2016) and because unrest detected by one of them might not be related to changes in the others (e.g., Heimissson et al. (2015); Delgado et al. (2016)). With these goals in mind, we carried out an Interferometric Synthetic Aperture Radar (InSAR) study focusing on three high priority volcanoes in the southern Andes of Chile.

The Southern Andes Volcanic Zone (SAVZ) (33°-46°S) of Chile and Argentina is one of the four distinct segments of the volcanic arc along the western margin of South America (Stern, 2004), and one of the most active volcanic provinces in Latin America, with 64 volcanic centers thought to be active during the Holocene (Siebert et al., 2010). The most active volcanoes of this province are Villarrica and Llaima, both with eruptions every ~3-6 years (Dzierma and Wehrmann, 2010), while the province as a whole has a time averaged rate of ~0.5 eruptions/year during the 20th century (Dzierma and Wehrmann, 2012). Holocene postglacial eruptions of the SAVZ volcanoes span the full compositional range from basalt to silica rich, and with volcanic explosivity indexes (VEI) up to 6 (Stern, 2004). The SAVZ is thus an excellent research place to understand the relation between of ground deformation and volcanic eruptions.

In this work we focus on Villarrica, Llaima and Calbuco volcanoes (Figure 1), the three most dangerous of the SAVZ according to SERNAGEOMIN (Lara et al., 2011),

<http://www.sernageomin.cl/archivos/Ranking-de-Volcanes.pdf>). In the absence of dense ground geodetic networks, we use satellite and airborne InSAR observations (e.g., Zebker et al. (2000); Dzurisin and Lu (2006); Simons and Rosen (2007); Lu and Dzurisin (2014); Pinel et al. (2014)) to establish the nature of ground deformation at each volcano. Our observations span most of the period between 2002 and 2015 -- including eruptions and periods of unrest at each volcano. We observe and model deformation at all three volcanoes, providing some of the first geophysical constraints on the location and dimensions of the plumbing systems, as remarkably little is known about their inner structure, mechanics of magma transport, storage, degassing and eruptive dynamics (e.g., (Bouvet de Maisonneuve et al., 2012; Bouvet de Maisonneuve et al., 2013); Witter et al. (2004); Palma et al. (2008); Castruccio et al. (2016)). As we do not always find clear evidence of pre-eruptive ground deformation, we discuss plausible reasons, including the model of open-closed volcanoes (Chaussard et al., 2013) to explain the complex relation between eruption and deformation at these edifices.

From the outset, we note that the application of currently available InSAR to volcanic edifices like the three studied here is challenging for several reasons. The steep slopes produce geometric distortions in spaceborne SAR images, vegetation and ice produces signal decorrelation (e.g., Zebker et al. (2000); Pinel et al. (2011)), and variations in water vapor and hydrostatic pressure that correlate with topography can introduce significant phase delays in the radar line of sight (LOS) that can be mistaken as ground deformation (e.g., Beauducel et al. (2000); Remy et al. (2003)). Given this context, our approach is to use data from all available InSAR spaceborne and airborne platforms spanning a range of wavelengths (X, C, and L bands, roughly 3, 6 and 24 cm) and viewing geometries for each volcano in order to best separate real ground deformation from other signals. Our goal is also to understand how radar wavelength, image swath width, and satellite/aircraft repeat interval impacts data quality under the environmental conditions of the SAVZ stratovolcanoes with an eye to assessing the utility of each type of observation for systematic monitoring. For example, it is known that decorrelation is more critical at shorter radar wavelengths (like X band) (Rosen et al., 1996), but X band data potential has not been properly assessed in the region -- to our knowledge it has

mostly been used in the SAVZ at volcanoes in the eastern part of the region or with less vegetation (Feigl et al. (2014); Delgado et al. (2016); (Lundgren et al., 2015b)) than the three volcanoes studied here. Further, to understand and possibly remove atmospheric artifacts on the interferograms, we use both empirical corrections and numerical weather models that have been shown to be useful elsewhere (e.g., Doin et al. (2009); Jolivet et al. (2011); Bekaert et al. (2015)). Based on the available data, we recommend a regional observation strategy that utilizes the unique capabilities of each satellite, considering the peculiarities of these three most dangerous volcanoes in the region.

2. Geological Background and Previous Work

2.1 Llaima volcano

Llaima (71.25°W, 38.70°S) is one of the most active volcanoes in the SAVZ, with more than 50 eruptions since the XVII century (Naranjo and Moreno, 2005). It is a large stratocone built on top of a post-glacial shield volcano, with a maximum elevation of 3179 m, made up by two NS oriented summits (the northernmost one is the main eruptive vent), and surrounded by more than 40 cinder cones in its W, N and S flanks. Llaima has been active since before the last glacial maximum and most of its erupted products have basaltic to andesitic-basaltic compositions, with low intensity Hawaiian and Strombolian historical eruptions. However, as the volcano is covered by large glaciers (~0.5 km³ of ice), it is particularly hazardous for the surrounding communities (Naranjo and Moreno, 2005).

The 2007-2009 eruptive cycle is the closest monitored to date at Llaima (Naranjo et al. (2009); Moreno et al. (2009)) and started on May 26 2007 with an overall increase in the seismicity above background levels and minor explosions and cinder emission. On January 1 2008, a Strombolian eruption that lasted 12 hours emitted an eruptive column that reached up to ~11 km over the volcano summit and with an erupted volume of ~0.0013 km³ (Ruth and Calder, 2014). The eruption was followed by Strombolian and Hawaiian eruptions between January 21-February 2 and February 2-13 2008 respectively. Activity restarted on July 2008 when 5 mixed Strombolian-Hawaiian eruptions were ejected followed by short periods of calm. The second large paroxysm of the cycle was a

mixed Strombolian and Hawaiian eruption that occurred on April 3 2009, lasted 72 hours and emitted three lava flows towards the W glacier (Figure 2) and an eruptive column that reached an elevation of 7 km, but to our knowledge no estimates of the erupted volume of this eruption are available. The volcano activity slowly waned until it ended in July 2009. The volcano seismic network recorded sudden increases in the real-time seismic-amplitude measurement (RSAM) a few hours or just before the eruptions, followed by a quick RSAM decrease as the eruptive activity waned (Basualto et al. (2009), Franco et al. (2015)). Petrological analysis of lava and tephra from historical eruptions, including the 2008 and 2009 events suggests that dikes of different magma batches are intruded across the NS oriented summits and that the dike volume controls the eruptive styles (Bouvet de Maisonneuve et al., 2012; Bouvet de Maisonneuve et al., 2013). The time scales of magma recharge are ~1-2 years to several months before the eruption (Bouvet de Maisonneuve, 2011) and magmas are likely stored at dike-like reservoirs at depths shallower than 4 km beneath the volcano surface (Bouvet de Maisonneuve et al., 2012; Ruth et al., 2016). Other unrest in the studied period include a small eruption on April 09-11 2003 with a VEI of 1-2 (Naranjo and Moreno, 2005).

Llaima is the only one of the three volcanoes that has been subject to previous detailed ground deformation studies. The 2007-2009 eruptive cycle was studied with ALOS data (Fournier et al., 2010), ENVISAT data (Bathke et al., 2011), and a reanalysis with both data sets plus independent estimates of precipitable water vapor (PWV) from MODIS and MERIS near infrared spectrometers (Remy et al., 2015). Fournier et al. (2010) and Remy et al. (2015) did not find unambiguous evidence for magmatic driven subsurface ground deformation except for a potential landslide located on the E part of the volcano likely triggered by the eruptive activity. Bathke et al. (2011) interpreted concentric fringes to reflect long term subsidence between 2003-2007 and coeruptive uplift before and during the January 1 2008 eruption. We further discuss the difference between these interpretations in the results and discussion sections.

2.2 Villarrica volcano

Villarrica (71.93°W, 39.42°S) is one of the most active volcanoes of the SAVZ with more than 50 historical eruptions since the 16th century (e.g., Lara and Clavero (2004),

Moreno and Clavero (2006)). It is an ice capped basaltic-andesitic stratovolcano, with a maximum elevation of 2847 m and the current stratocone is built on top of an older collapsed edifice. Since the last eruptive episode in 1984, the volcano crater has been filled with an actively degassing lava lake, 200 m in diameter (e.g., Witter et al. (2004); Palma et al. (2008); Moussallam et al. (2016)). The lava lake depth and explosions are correlated with the seismic tremor magnitude and the amount of outgassing and style of bubble bursting (Palma et al., 2008). The volcano erupted basaltic andesites from the summit crater on March 3 2015 03:08 local time and the eruption was preceded by a continuous increment in the background seismicity and small explosions of the lava lake (OVDAS, 2015). The eruption was transitional from strong Strombolian to Hawaiian, lasted 55 min and partially covered the crater rim with pyroclastic material (Naranjo, 2015) (Figure 2). The eruption ejected spatters ~1.5 km over the volcano crater and a column of gases and ash with an elevation of ~6-8 km during the highest intensity peak, while the seismicity decreased to levels lower than before the eruption (OVDAS, 2015). Smaller Strombolian eruptions were later produced on March 17 and 30 2015 (OVDAS, 2015). The total erupted volume of the March 3 2015 eruption is $0.0047 \pm 0.001 \text{ km}^3$ (Bertin et al., 2015)

2.3 Calbuco volcano

Calbuco (72.61°W, 41.33°S) is an andesitic stratovolcano with an elevation of ~2003 m. Most of its Holocene activity has been explosive sub-Plinian to Plinian, including a large sector collapse after the last glacial maximum and the eruption of lavas and domes (Selles and Moreno, 2011). There is recorded evidence of at least 12 historical eruptions, and its largest historical eruptions occurred in 1893-1895, when a lava dome was formed inside the collapsed structure, and with the most recent large and minor eruptions in 1961 and 1972 respectively (Selles and Moreno, 2011). The volcano was monitored by two seismometers since 2009, with the closest station 5 km to the west, and a tiltmeter 4 km west of the volcano. The eruption started on April 22 2015 18:04 local with little warning as earthquakes increased over background levels only ~3 hours before, with no clear precursors 15 minutes before the onset and with no pre eruptive deformation detected from the tiltmeter (Valderrama et al., 2015). The April 22 eruption was sub-Plinian (VEI 4), lasted ~1.5 hours and ejected a ~15 km height eruptive column of andesitic (57%

SiO₂) and basaltic-andesite (54-55%) composition (Romero et al. (2016); Van Eaton et al. (2016)). A second eruption started on April 23 2015 01:08 local time and lasted for 6 hours with a column that reached ~15 km height, and with earthquakes with maximum M_L magnitude of 3.6. A smaller column, with an elevation of ~2 km, was ejected one day later at 23:39 local time, and a third large eruption with a steam-driven column with an elevation of ~4 km that lasted ~2 hours occurred on April 30. Total erupted volumes estimates are 0.27 ± 0.007 (Romero et al., 2016), 0.56 ± 0.28 (Van Eaton et al., 2016), and 0.38 km^3 (Castruccio et al., 2016). The erupted volumes during the April 22 and 23 eruptions are 0.103 ± 0.0027 and $0.167 \pm 0.0043 \text{ km}^3$ respectively (Romero et al., 2016).

3. InSAR processing and modeling

InSAR data and processing details are described in the supplementary material, hence we only briefly describe the methods here. We use all the available ERS-2, ENVISAT and ALOS stripmap SAR data at the volcanoes spanning October 1997-December 2000, December 2002-March 2012, and December 2011-March 2011, respectively, as well as some RADARSAT-2 (hereafter RS2), TerraSAR-X (TSX), COSMO-SkyMed (CSK), Sentinel-1A (S1A) and ALOS-2 data acquired between December 2012 and June 2015 (Table 1, Figure 1). We also use L band UAVSAR (Uninhabited Aerial Vehicle Synthetic Aperture Radar) interferograms processed and provided by NASA/JPL between 2013 and 2015. ERS-1/2 data coverage at both Villarrica and Llaima is very sparse with only a single acquisition in 1997 and five scenes in late 2000 (Stevens and Wadge, 2004) – the interferograms have low coherence so are not discussed in detail. ENVISAT observations include data from the nominal mission between December 2002 and October 2010, as well as images acquired in the extended mission between November 2010 and March 2012. The latter data cannot be combined with the former, but using both has the advantage that during the extended mission, images were almost continuously acquired every 30 days with 12-18 images per volcano. In contrast, ENVISAT nominal mission tracks contain 6-7 images per year between 2003 and 2005, but no more than 3 images per year between November 2005 and October 2010 (Table 1). ENVISAT ScanSAR subswaths can be combined with stripmap images (Ortiz and Zebker, 2007) to fill gaps in the latter catalog (Pepe et al., 2011) but as there are only 16 ScanSAR scenes and only

two after November 2004, the poor data temporal sampling is not much improved and so the data were not analyzed further. Regarding TSX, stripmap data has only been systematically acquired at Calbuco since July 2016 and spotlight mode has been acquired at both Llaima and Villarrica since February and May 2012 respectively, with scenes every 11 – 22 days (1-2 orbital cycles). We processed a few TSX scenes acquired between March and May 2015 at Villarrica to compare with signals observed in CSK data. We note that Calbuco has less than half and one third of the ALOS and ENVISAT data sets respectively, compared to either Villarrica or Llaima. Further, a data gap exists at Calbuco between the last ENVISAT image in March 2012 and the first RS2 acquisition in December 2012, and neither CSK nor TSX acquired data suitable for either stripmap or spotlight interferometry before the 2015 eruption.

For areas with sufficient ALOS, ENVISAT extended mode, CSK and S1A data (at least 10-20 interferograms) we calculate time series of deformation (Berardino et al., 2002). We also try a variety of techniques to account for the persistent atmospheric phase delays observed in the volcanoes (e.g., Beauducel et al. (2000); Froger et al. (2007); Chaussard et al. (2013); Jolivet et al. (2014); Remy et al. (2015), Supplementary material). When observed, deformation signals were jointly inverted from several interferograms using standard algorithms for data downsampling and covariance matrix estimation (Lohman and Simons, 2005) as well as standard solutions for pressurized sources in a linear elastic half space ((McTigue, 1987); (Okada, 1985); Yang et al. (1988)) and with topographic corrections (Williams and Wadge, 1998).

4. Results

We describe here InSAR data that span eruptions and periods of known unrest including the 2007-2009 Llaima eruptive cycle, and Villarrica and Calbuco during their 2015 eruptions. The rest of the data sets do not show unambiguous evidence of ground deformation and hence are described in detail only in the supplementary material.

4.1 Llaima volcano

Both atmospheric corrected and uncorrected 2007-2011 ALOS time series (Figure 3) show a LOS increase (hypothetical subsidence), also observed by Remy et al. (2015). ENVISAT interferograms that overlap with the ALOS data show LOS decrease (hypothetical uplift) (Figure 4), with amplitudes up to ~6 cm. The analysis of whether these signals are ground deformation or atmospheric effects will be evaluated in the discussion section. The ALOS LOS increase trends are interrupted by a burst of LOS decrease (uplift) in early 2009 as described in the next section.

4.1.1 Pre eruptive inflation before the April 3rd 2009 eruption

A distinct transient burst of uplift is observed before the April 3 2009 eruption in the two independent ALOS time series in the same part of the volcano (**Figure 3, Figure 5**). The uplift is an outlier in the overall trend in the time series and is above the ± 7 cm uncertainty inferred for interferograms at Llaima volcano (Remy et al., 2015). Further, the uplift signal appears in only three interferograms calculated with two independent SAR acquisitions (Supplementary Material and **Table 2**) and is not correlated with topography as sometimes observed for signals of atmospheric origin. Thus we interpret it as real ground deformation instead of an atmospheric signal. Remy et al. (2015) also observed this signal in the path 117 interferogram (**Figure 5d, Table 2**) and noted that the pair in question is not affected by a significant atmospheric phase delay in the volcano but did not interpret it as ground deformation. The signal is not observed in ENVISAT interferograms that cover the April 3 2009 eruption (**Figure 4**) but the former did not acquire SAR images ~1-2 months before the eruption and the signal was presumably canceled out by post eruptive subsidence with net zero cumulative displacement. We interpret this signal as ground uplift most likely related to pre-eruptive magma intrusion before the April 2009 eruption, in agreement with time scales of magma intrusion on the order of several months to ~1-2 years interpreted on the basis of geochemistry (Bouvet de Maisonneuve, 2011). Had we observed the signal in a single interferogram as Remy et al. (2015) did, the interpretation as ground uplift would be more suspect. The non-optimal data availability hampers our ability to assess the uplift event time dependence, duration and precise timing, as it was temporally aliased by the almost complete lack of SAR acquisitions between July 2008 and February 2009.

To model the putative uplift signal before the 2009 eruption, we selected 3 interferograms (Table 2), masked most of the interferograms far from the volcano as well as the potential landslide signal (Fournier et al., 2010), but left enough non-deforming areas to estimate the data covariance matrix. As the deformation observed before the April 3 2009 eruption is elongated, a symmetrical source (like a single Mogi model) can be ruled out. As a joint inversion for a pressurized ellipsoid predicts an unrealistic small aspect ratio, we focused on the tensile dislocation model. We tested a variety of inversions with different combinations of interferograms, with and without the empirical atmospheric correction and the volcano topography taken into account in the source model. We find that because the deformation is larger in the path 116 interferograms than the path 117 interferogram, the inverted sill opening is ~ 8 cm larger, but the master scene on the former interferograms was acquired earlier than the latter. Given the limited number of SAR acquisitions, it is not possible to determine if the difference between the two paths is related to time variable deformation or to atmospheric effects. Hence, in the absence of further data to reduce the effect of the phase delays, we show the inversion results calculated with the three interferograms uncorrected for phase delays and for topographic relief that fits both tracks, but is not optimal for either. The best-fit model predicts a sill like geometry with the centroid depth of $\sim 5.3 \pm 0.6$ km beneath the volcano base (~ 1700 m) (Table 3) and a volume change of 0.0093 ± 0.0078 km³, which we compare to the petrologically inferred depth in the discussion.

4.1.2 Deformation of non magmatic origin

Fournier et al. (2010) described a LOS increase signal in the E part of the volcano observed in both the ALOS and ENVISAT (Figure 4) data sets and interpreted as a potential landslide, but such process was not observed in that area. An alternative explanation involves flank instability inferred from the occurrence of new small flank vents where small explosions were sourced over this flank [Hugo Moreno, personal communication]. Hence, we re-interpret this geodetic signal as being produced by flank instability after the January 1 2008 eruption. Although our dataset is significantly larger than the one analyzed by Bathke et al. (2011); Fournier et al. (2010) or Remy et al. (2015), the sparse ENVISAT/ALOS image catalog in early 2008 hampers our ability to

provide better constrains on the flank instability timing, which occurred after December 7 2007, most likely following the January 1 2008 eruption, and before March 4 2008.

4.2 Villarrica Volcano

The co-ruptive CSK and S1A time series spanning December 2014 to April 2015 (Figure 6) show both LOS increase and decrease (hypothetical subsidence and uplift) respectively, but the signals have different signs for similar time periods. The analysis of whether these signals are ground deformation or atmospheric effects will be evaluated in the discussion section.

4.2.1 Post eruptive inflation after the March 3rd 2015 eruption

CSK interferograms calculated with several independent SAR images that span mid April to mid May 2015 (Figure 7, Table 4), show a persistent uplift signal located 5 km SE of the volcano, near the Holocene caldera rim, with maximum amplitudes between 4 and 6 cm. The uplift signal is not shown in Figure 6 because it was not possible to calculate coherent small baseline interferograms to include it in the CSK time series and due to the large magnitude of non-stationary topography correlated phase delays in the S1A interferograms. The amplitude scales with the covered time span consistent with a time dependent process, but there is not enough data to characterize the temporal evolution. The signal was detected by OVDAS on four cGPS stations and related to an increase in volcano tectonic seismicity (Córdova et al., 2015). The signal is not correlated with topography and appears in the same area in interferograms with independent acquisitions, but is absent in ascending TSX spotlight interferograms (Supplementary material) that cover only a small fraction of the deforming area. In order to model the uplift signal, we estimate and remove atmospheric phase delays correlated with the topography by inverting a Mogi source (Córdova et al., 2015) with a topographic correction (Williams and Wadge, 1998), and then jointly invert the best six CSK interferograms. DEM errors produced by the retreat of the glacier that covers the volcano and close to the inferred uplift area were cropped so they will not bias the source model. The inversion results (Table 5) show that a source located ~4.2 km beneath sea level can reproduce the observed uplift signal, ~2 km deeper than the cGPS model with a cumulative volume change of 0.0075 km^3 during the uplift period. The discrepancy between the InSAR –

GPS model can be explained because the sparse GPS network does not capture the full extent of the deformation signal, therefore the InSAR inversion is modeled by either a deeper source or a source with a larger strength, a slight difference in the time period covered by GPS and InSAR, or because the InSAR model is biased by using a single component of deformation. In the absence of further independent data sets we consider these explanations for the difference between the InSAR-GPS models equally likely.

4.3 Calbuco volcano

4.3.1 Co-eruptive subsidence during the April 22-23 2015 eruptions and localized atmospheric signals?

Sentinel-1A interferograms that span the April 22-23 2015 eruptions show a maximum subsidence of ~12 cm in the W part of the volcano for the ascending data (Figure 8), and a signal of similar amplitude in the E part of the volcano for the descending one, which is more decorrelated due to ash deposition during a longer time span. An ascending Sentinel-1A interferogram that spans the April 22, 23 and 30 eruptions shows a signal of the same amplitude as those that only span the first two eruptions. The subsidence signal is also observed in an ALOS-2 ascending stripmap (available at http://www.eorc.jaxa.jp/ALOS-2/en/img_up/dis_pal2_ch1-volc_20150429.htm) and in descending ScanSAR interferograms (not shown). 1-day CSK descending interferograms calculated with images acquired between ~24 and ~72 hours after the April 22 2015 eruption show contrasting signals (Supplementary material). The first 1-day pair shows range increase (apparent subsidence) in the S part of the volcano and uplift in the N volcano flanks, but not in the edifice itself, both signals of ~2 cm, while the second 1 day pair shows uplift in the volcano and subsidence in its N flank, both signals with an amplitude of ~3.5 cm. Given the lack of complementary data, it is unclear if these signals in the 1-day pairs correspond to real ground deformation.

The coeruptive subsidence signal in the Sentinel-1A interferograms can be modeled by a prolate pressurized spheroid located ~1 km SW of the volcano summit at a depth of ~8 km, or alternatively by a point source ~5.5 km SW of the volcano at a depth of 10.7 km

(Figure 8, Table 6, **Table 7**). Nevertheless, residuals are large as neither model can properly model both ascending and descending data. On the other hand, the subsidence signals observed in the 1-day CSK pairs, if real, are neither co-located with lahars (deposited over a smaller area than the phase anomaly or the eruptive plume (which was ejected towards the E of the volcano as observed in GOES-13 (Romero et al. (2016), Van Eaton et al. (2016)), MODIS and EO-1 satellite imagery).

As the co-ruptive deflation signals were observed in the Sentinel interferograms but not in the 1-day CSK pairs, the volcano magma chamber deflated during the extent of the April 22-23 eruptions, in agreement with the tiltmeter records (Valderrama et al., 2015). The deformation is negligible for the April 30 eruption as evidenced by interferograms that only span the latter eruption. The fact that none of the source models can properly predict both the ascending and descending interferograms implies that the source is more complex than the simple models used here (Nikkhoo et al., 2016) and a different source model may be required – but all available models are consistent with a source depth between 8-11 km.

To compare the volume of erupted material with that inferred from the geodetic model, we use the spheroid source model as a proxy of the magma chamber volume change because it has a smaller root mean square compared with the point source (**Table 7**). The chamber volume change of $\sim 0.07 \text{ km}^3$ can be converted to erupted volume by means of

the formula $\frac{V_e}{V_c} = \frac{\rho_M}{\rho_e} \left(1 + \frac{m}{c} \right)$ (Mastin et al., 2008) with V_e the erupted volume, ΔV_c

the magma chamber volume, ρ_M and ρ_e the chamber and erupted magma densities, κ_C the magma compressibility, and κ_m the magma chamber compressibility. Amoruso and Crescentini (2009) showed that a prolate spheroid with an aspect ratio of 2.34 as in Calbuco has a chamber compressibility very similar to $3/4G$ with G the medium shear modulus, and characteristic of a spherical source, hence we use the latter value for the calculation. As no seismic velocity or volatile contents estimates of the erupted products are available for Calbuco, we use literature values of $G = 10 \text{ GPa}$ for somewhat fractured crust (Segall, 2010), $\kappa_m = 2.5 - 5 \times 10^{-10} \text{ MPa}^{-1}$ for andesites (Mastin et al., 2009) and

assume that ρ_M equal to ρ_e . These figures yield a ratio of erupted volume versus magma chamber volume change between 4.3 to 7.6, and erupted volumes of 0.28 – 0.495 km³, within uncertainties of the actual erupted volumes (Van Eaton et al. (2016), Romero et al. (2016), Castruccio et al. (2016)).

5. Discussion

5.1 Discriminating deformation from atmospheric phase delays

The coeruptive Llaima and Villarrica data sets require a careful assessment of whether there could be real ground deformation or not (Remy et al., 2015). Below we describe a more detailed analysis of each volcano in turn.

5.1.1 Lack of deformation at Llaima during the January 2008 eruption

For the early 2007 - mid 2008 period, the six coeruptive Llaima ENVISAT interferograms show LOS decrease (**Figure 4**), although of different amplitude, while the ALOS path 116 time series shows a slight LOS increase and the ALOS path 117 time series shows effectively no cumulative deformation when corrected for atmospheric effects (**Figure 3**). As all the data sets show different results, we conclude that no InSAR detectable subsurface magma driven ground deformation occurred during the 2008 eruptions and that all the observed patterns of LOS decrease in the ENVISAT data were produced by tropospheric phase delays -- in agreement with Fournier et al. (2010) and Remy et al. (2015), but differing from Bathke et al. (2011). Indeed, the mean velocities from the ALOS time series in 2007-2008 are smaller than the assumed ~2.5 cm/yr ALOS time series accuracy (Supplementary material). A synthetic Mogi model projected into ENVISAT and ALOS LOS, and that takes into account both the topography and magma compressibility of the erupted tephra of the January 1st 2008 eruption (Ruth and Calder, 2014) predicts that an inflating source located 7 km beneath Llaima summit (Bathke et al., 2011) produces at most 2 mm of LOS subsidence (not shown). Such signal is one order of magnitude below the uncertainty of our time series for secular rates and interferograms for transient signals and is thus not resolved in our data.

5.1.2 Lack of deformation during the 2015 Villarrica eruption

The CSK / S1A time series show ground velocities of opposite sign and with random signals during, before and after the eruption. The erupted volume of the March 3 2015 eruption is equivalent to $0.002 \pm 0.0004 \text{ km}^3$ of magma, if compressibility for a mostly degassed basalt is taken into account (e.g., Witter et al. (2004); Segall (2010)). The deflation signal produced by the evacuation of that volume is not evident in the time series (Figure 6) as a deflating source located beneath the volcano summit at the same depth of the deeper source responsible for the 1971 eruption (Morgado et al., 2015) produces less than 1 cm of co eruptive subsidence. The signals observed in the S1A and CSK time series have larger amplitudes than the predicted subsidence and do not show systematic signals with the same amplitude and located in the same areas. Hence, we conclude that the available data set is not indicative of unambiguous evidence for pre-eruptive inflation and co-eruptive deflation, in agreement with the available GPS records (Córdova et al., 2015).

5.1.3 Lack of deformation during the April 30 2015 Calbuco eruption

Neither CSK nor S1A data show unambiguous deformation signals related to the third eruption in the April 2015 sequence. The lack of ground deformation could be related to the fact that the eruption products have low juvenile contents indicative of a steam driven eruption with little involvement of magma (Van Eaton et al., 2016) and had a volume that was an order of magnitude smaller volume than the April 22-23 eruptions [Daniel Bertin, personal communication]. Hence the eruption was not likely produced by the evacuation of magma from a chamber that could produce ground deformation.

5.2 Implications for magma plumbing systems

We provide the first geodetic measurements of ground deformation confirmed by multiple datasets at these the most active and dangerous volcanoes in the SAVZ and some of the first inferences of any kind about the depth and location of magma chambers that may feed the eruptions. We discuss each in turn.

We interpret that the 2009 eruption at Llaima was preceded by the inflation of a sill at a depth of $\sim 5.3 \pm 0.6 \text{ km}$ beneath the volcano base on the western side of the volcano. This geophysical depth is at the extreme of the petrological inferences of the magma chamber

depth that fed the Llama eruptions (Bouvet de Maisonneuve et al., 2012), but both estimates barely overlap. If potential systematic errors in the geophysical estimate such as heterogeneity of the elastic structure beneath the volcano (Masterlark, 2007) are taken into account, both the InSAR and petrology estimates are in agreement as they show a relatively shallow magma chamber. Because there is no net deformation in interferograms that span the eruption, we infer that the sill must have emptied during the eruption with the same pattern and amplitude of ground deformation as seen in the pre-eruptive intrusion. The intrusion and extrusion of magma or the pressurization and then depressurization of gas could cause the ground deformation, but to our knowledge no estimates of the erupted volumes are available for comparison with the sill volumetric change of $0.009 \pm 0.007 \text{ km}^3$.

At Villarrica, the ground uplift source after the March 2015 eruption is inferred to be located ~5 km SE of the volcanic edifice at a depth of ~4.2 km below the sea level and related to an increase in volcano tectonic seismicity in the same area (Córdova et al., 2015), but the relation of this deformation source to the volcanic plumbing system is unclear. The 4.2 km geophysically inferred depth of the magma chamber is at the lower end of the depth inferred from petrology mentioned above ((Witter et al., 2004), Morgado et al. (2015)), but is clearly deeper than the depth of the seismic source which may be related to conduit processes (Richardson and Waite, 2013). No evidence for sources of hydrothermal origin have been recorded at Villarrica (Moreno and Clavero, 2006), hence we suggest that the inverted source is of magmatic origin, although with the limited data sets, the relation of this inflation source with the March 3 2015 eruption is unclear. Perhaps the deformation is related to the eruption either by a refilling of the Villarrica magma chamber after the area was evacuated by the eruption or a pressurization of the magma chamber caused by devolatilization driven by the expulsion of magma in the eruption. If so, why is there a delay of several weeks between the end of the eruption and the observed uplift and the location of the inflation source with respect to the volcano crater? However, such connection between the sources by a hypothetical dike (not shown) does not predict the uplift signal in the few coherent areas. Further geophysical investigations are necessary to test for links between the inflationary source and the

conduit processes that characterize the current activity at Villarrica (e.g., Witter et al. (2004); Palma et al. (2008); Moussallam et al. (2016); (Richardson and Waite, 2013)).

The Calbuco subsidence occurred during the first and second eruptions on 22 and 23 April 2015, caused by a source at ~8-11 km depth below the summit or slightly to the west depending on the source geometry (Table 6 and Nikkhoo et al. (2016)). This depth is about twice as deep as Villarrica and Llaima modeled sources and is one of the deepest compared with sources modeled from geodetic data at other volcanoes in the SAVZ (e.g., Wicks et al. (2011); Feigl et al. (2014); Delgado et al. (2014); Jay et al. (2014); Velez et al. (2015); Delgado et al. (2016)). The main differences between Calbuco and both Villarrica and Llaima are the magma compositions as the former is andesitic (Selles and Moreno, 2011) and the latter are basaltic-andesitic edifices (Moreno and Clavero (2006), Naranjo and Moreno (2005)). The neutral buoyancy hypothesis (Walker, 1989) predicts that basaltic magmas should be stored at deeper chambers compared with more silicic magmas for similar ambient crust, hence the Calbuco chamber should be shallower than those beneath Llaima and Villarrica, but this is not consistent with our geodetic observations. The three edifices have similar stress regimes (Cembrano and Lara, 2009) hence it cannot explain the differences between the depth of the different modeled sources (Chaussard and Amelung, 2012). Tomographic and thermal models to compare the shallow plumbing systems and the crustal structure of the three volcanoes are not available, but we speculate that the hotter basaltic-andesitic magmas and more frequent eruptions at Villarrica and Llaima create a warmer thermal profile than at Calbuco that could allow for the shallower observed magma chambers. On the other hand, Castruccio et al. (2016) suggested that the eruption was triggered by either volatile exsolution or a small magma intrusion into the base of the magma chamber and with the same composition of the latter. We consider the dike intrusion a less likely mechanism than volatile exsolution because synthetic models for a dipping dike (not shown) with similar volumes as those from the source models do not predict the co-eruptive interferograms.

5.3 What does the lack of ground deformation associated with some eruptions mean?

In addition to our observations of deformation mentioned above, observations of null deformation during certain time periods provide some constraints on magma movements (or lack thereof) at these three volcanoes. But a key question is could the lack of observed deformation be due to the limited spatial and temporal sampling of the InSAR observations? This is an issue of special concern for ALOS data due to its 46 days orbital period and the satellite orbit reset in early 2009. For example, we observed deformation at least 1 and half months before the April 2009 Llaima eruption (Figure 5), but interferograms that span the eruption show no net deformation (Figure 3; Figure 4) indicating co-eruptive subsidence that canceled the pre-eruptive inflation. So perhaps the nearly equal balancing of inflation before and after eruptions could explain the lack of deformation associated with the March 2015 Villarrica eruptions or the 2008 Llaima eruptions. On the other hand, there are interferograms up to one day before the April 22 2015 Calbuco, 24 days before the January 1 2008 Llaima and 4 days before the March 3 2015 Villarrica eruptions that do not show any pre-eruptive inflation – so that lack of deformation result is robust within the limits of the atmospheric noise and coherence in those images. Deformation below the noise level and within decorrelated areas would of course be hidden, and we address observing strategies in the next section to reduce noise and increase coherence.

A useful model for considering the relation between eruptions and ground deformation is the classification by Chaussard et al. (2013) of open and closed volcanoes – closed systems are volcanoes with ground deformation signals of subsurface magmatic origin, while those with a lack of those signals are considered open systems. This is a specific definition for ground deformation purposes and is used as such in the following sections unless it is explicitly stated. A magma chamber beneath a closed volcano can be pressurized by volatile exsolution or magma intrusion, as the conduit that connects it with the surface is obstructed by a solid plug or pyroclastic material, while chamber pressurization at open systems is relieved by passive degassing, lava dome growth, lava ejection and minor explosions. At such edifices, eruptions might be a consequence of

subtle magma chamber changes (Chaussard et al., 2013). This might reflect the presence of a permanent or semi permanent open conduit, which may result in deformation only near the volcano summit where InSAR data tends to be systematically decorrelated at the three volcanoes considered here. However, there are several limitations to this model. For example, a volcano with a conduit blocked by a pressurized viscous solid plug can produce deformation but it can only be recorded by instruments located a few hundreds meters from the conduit (Albino et al., 2011). This type of deformation can be aliased by poor spatial sampling but the lack of measured deformation does not imply that the volcano has a physically open conduit. A counterexample of the open-closed model is Kilauea volcano with physically open conduits but with ground deformation with wavelengths of several km and during multiple eruptions (e.g., Baker and Amelung (2012); Poland et al. (2014); Patrick et al. (2015)).

A different model for volcanoes with open conduits with either permanent or semi permanent degassing is that passive degassing may lead to endogenous growth due to magma accumulation beneath a volcanic edifice (Francis et al., 1993) and therefore the intrusion growth should produce ground deformation. This model might apply to Villarrica and Llaima, as both are systems that have permanent or semi permanent passive degassing (Mather et al. (2004); Witter et al. (2004); Witter and Calder (2004); Gurioli et al. (2008); Palma et al. (2008); Palma et al. (2011); Bredemeyer and Hansteen (2014); Moussallam et al. (2016)). We assess the minimum depths where such sources could be located from SO₂ emissions under the assumption that they produce maximum ground deformation beneath the ± 2.5 cm/yr detection rate for the ALOS time series (e.g., Ebmeier et al. (2013)) by means of the formula $V = u_z d^2 / (1 - \nu)$ (McTigue, 1987) with ΔV the predicted volume, u_z the minimum detection threshold, d the source depth and ν the Poisson ratio equal to 0.25. Witter et al. (2004) used correlation spectrometry measurements in the austral summer of 2000 and 2001 to estimate that 2.0 ± 1.2 m³/s of magma are degassed from Villarrica volcano, equivalent to a yearly volume flux of 0.063 ± 0.037 km³/yr. If an equivalent volume of magma is intruded into a spherical magma chamber beneath the volcano summit and corrected by a factor of 2.3 to take into account magma compressibility (Segall, 2010) such a source should lie between 10 and 20 km

beneath Villarrica (Supplementary material). SO₂ fluxes have also been calculated at Llaima (Bredemeyer and Hansteen, 2014; Mather et al., 2004), but in the absence of the sulfur lost from the melt, a figure needed to convert SO₂ mass flux into volume flux (Kazahaya et al., 1994), we did not calculate the inferred reservoir depth. Witter et al. (2004) noted the lack of secular ground deformation at Villarrica for such a large volume change in a hypothetical magma chamber and concluded that magma convection driven by dense degasified magma batches that sink back into the conduit (Kazahaya et al., 1994) is the most likely heat and volatile transport mechanism. This is in agreement with the location of a stable seismic source 1 km beneath the volcano crater and inside the conduit related to the lava lake outgassing (Richardson and Waite, 2013). Although the open conduit and the endogenous growth models are not mutually exclusive, when both are compared with the geodetic and degassing data, the lack of secular ground deformation between 2002 and 2015 at Villarrica is most likely explained by the former. On the other hand, the open-closed volcano model might apply for the 2007-2009 Llaima eruptive cycle as well, as aerial observations several days before the April 3 2009 eruption showed that the conduit was obstructed with pyroclastic material (OVDAS, 2009) but similar observations were not available before the January 1 2008 eruption.

It has been observed that the 1957, 2008 and 2009 Llaima eruptions (Naranjo and Moreno (2005), Naranjo et al. (2009), Bouvet de Maisonneuve et al. (2012)) as well as the 1948-1949 (Casertano, 1963a; Casertano, 1963b), 1963-1964 (Naranjo and Moreno, 2004) and 1971 (Moreno, 1993) eruptions at Villarrica erupted lava and gas from dikes and fissures aligned with the N and S Llaima summits and close to the Villarrica summit. Depending on the size of the dike intrusion, the ground deformation signature may not be detected in the available data. For example, a dike that opens 1 m and aligned with the Llaima volcano vents produces displacements in the limited coherent areas within the atmospheric noise amplitude (Supplementary material). However, larger dike intrusions at stratovolcanoes tend to produce LOS surface displacements larger than ~0.15 m (e.g., Currenti et al. (2011), Wauthier et al. (2012); (Lundgren et al., 2015a)) and above the InSAR detection threshold, but we cannot constrain the minimum amount of dike opening to be geodetically detected because the opening of these structures was not

measured. It is also possible that many dike intrusions, like those described earlier are not likely to generate signals detectable with the available InSAR platforms because they occur on areas of the edifices that are systematically decorrelated. This motivates developing InSAR observing strategies that produce observations on the edifices (see final section).

The open-closed conduit model cannot explain the lack of pre-eruptive ground deformation up to 1.5 days before the Calbuco eruption because there was not evidence of an open conduit with either permanent or semi permanent degassing. The lack of pre-eruptive deformation could be related to the fast ascent of highly compressible gas-rich magmas that leave no geodetic overprint in the available InSAR data (e.g., Ebmeier et al. (2013), Biggs et al. (2014)), as in Chaitén (Fournier et al., 2010; Wicks et al., 2011) and Mt. St. Helens volcanoes (Poland and Lu, 2008) or magma recharge at rates below the detection threshold or during periods with no InSAR observations. Indeed if all the magma that was erupted was intruded in the same reservoir with a secular rate since the previous eruption in 1972, the expected ground uplift LOS velocity is ~ 2.8 mm/yr, 1 order of magnitude below the accuracy of the time series and not resolvable with the available data.

In summary, a variety of processes including temporal aliasing, volcanoes with open conduits, deformation that might only be detectable in areas likely to be systematically decorrelated, and signals below the detection threshold can be responsible for the lack of deformation at the studied volcanoes. All these alternatives must be further explored before a volcano with a complicated relation of eruption and ground deformation, with persistent atmospheric phase delays, and with a lack of measurements near the conduit can be classified as either an open or closed system.

5.4 Coherence comparison between X, C and L band data

To develop more effective satellite monitoring in the SAVZ, we compile observations of InSAR data quality (InSAR coherence) from different seasons, repeat intervals, and radar wavelengths in Table 8. Although direct comparison of the different datasets is difficult because of variations in data availability, it is rare to have these observations for different

seasons and time periods. Another caveat is that our analysis does not consider the use of persistent scatterers (PS) (Hooper et al., 2007).

InSAR coherence is broadly similar at Llaima and Villarrica (they are less than 50 km from each other), but is much lower at Calbuco, which is located ~300 km farther S and closer to the ocean in a more humid area. However, coherence in ENVISAT nominal mission interferograms was sufficient on Llaima lava flows for more than 4 years, but not at Villarrica due to the higher slopes and more vegetation. Coherence is higher in the ENVISAT extended mission interferograms at both volcanoes because images were acquired more frequently and they have HH polarization instead of VV of the ENVISAT nominal mission consistent with results from Mt. St. Helens comparing RADARSAT-1 HH data with both ERS and ENVISAT VV data (Poland and Lu, 2008). Volcano size is important in coherence, as smaller edifices such as Calbuco or Lonquimay decorrelate faster than larger ones and are only coherent on one side of the volcano (Supplementary material).

Sentinel-1A/B observations are routinely collected every 24 days (at the time of this writing in February, 2017) at all three volcanoes except during the 2015 eruptions when the repeat period was temporarily reduced to 12 days at Calbuco and Villarrica. We find that 24 days is not always short enough for interferograms with a posting of ~30 m to remain coherent in the vegetated areas that surround the volcanoes, hence the repeat period should be reduced to at least 12 days. These observations beyond the volcano edifice are essential to separate real deformation signals at the volcano from atmospheric noise as well as to detect magmatic deformation that can occur at several tens of km from the volcano (Henderson and Pritchard, 2013).

As many historical eruptions at Llaima and Villarrica have been from eruptive fissures near the summits (Naranjo and Moreno, 2004; Naranjo et al., 2009), it is important to assess the best suited InSAR data sets to study this type of ground deformation. Table 9 summarizes the maximum temporal baseline for interferograms to remain coherent in the summits. At Llaima, RS2 and CSK interferograms from a single orbital cycle are mostly

decorrelated in the glacier-covered areas, but the summit seems to be coherent (Supplementary material). At Villarrica, the only data sets that are coherent over the glacier are 2-days UAVSAR and 1-day CSK interferograms that show evidence of both widespread glacier movement and DEM errors, although coherence is not sustained over most of the glacier for X band (Figure 9). Hence the only option to image these areas with the available platforms is to use 1-day CSK pairs with incidence angles higher than 30° to avoid potential SAR layover and foreshortening. Indeed, these interferograms have been shown to remain coherent over the Bárðarbunga ice-covered caldera with ground velocities as high as 0.6 m/day (Riel et al., 2015; Sigmundsson et al., 2015). Nevertheless, these data sets are not tasked continuously and baselines are not always optimal for interferometry. The presence of ice implies that continuously updated DEMs are required, and with a high resolution if the target is the volcano conduit (Salzer et al., 2015).

5.5 Satellite Monitoring Strategies

In summary, what is the best approach for monitoring these three most dangerous volcanoes in the SAVZ with InSAR, given the satellites currently available and the fast decorrelation in the area? To catch possibly short lived precursors and mitigate temporal decorrelation, in particular with X band data, observations during every satellite overflight would be desired and from platforms and beams that image multiple edifices, in order to use empirical corrections that correlate phase and topography to mitigate atmospheric phase delays. During the winter months (i.e., interferograms in the months June to October), collecting data during every overflight is still useful -- coherence on the edifice and the surrounding area is reduced, depending on the satellite repeat interval and radar wavelength, but we have found useful coherence in some X and C band winter pairs (Table 8). There is a trade-off between having high spatial resolution on these three volcanoes and having a wide enough image to capture deformation near the edifice and include multiple edifices in order to use empirical corrections that correlate phase and topography to remove atmospheric errors. This is a particular complication of X band data because of the small area of stripmap swath ($\sim 50 \times 50 \text{ km}^2$), and more so for TSX spotlight swaths ($\sim 11 \times 11 \text{ km}^2$). Despite the success of the latter mode to detect deformation produced by very shallow sources near volcano conduits (Salzer et al.,

2015), we suggest other modes of observation at Llaima and Villarrica from this satellite. Some signals such as the potential flank instability at Llaima and the post eruptive inflation at Villarrica are not completely imaged by its small swath, and its 11-day repeat period is not short enough to mitigate systematic decorrelation due to the glaciers on top of the volcanoes. Hence we suggest using C and L band data for regional scale monitoring and X band data for volcanic crisis when more frequent acquisitions are required. Further, frequently updated high-resolution DEMs possible from TanDEM-X and optical stereo imagery should be collected at these volcanoes.

6. Conclusions

We use multi-satellite X, C and L band InSAR observations at Villarrica, Llaima and Calbuco volcanoes in the SAVZ, and show evidence of ground deformation, periods with no clear deformation signal with and without eruptions, and provide guidance on future observing strategies for these three most dangerous volcanoes in Chile. Specifically:

1. We detect likely ground deformation at all three volcanoes:

Llaima: Pre-eruptive uplift before the April 3 2009 eruption from a sill-like source at about 5 km depth on the west side of the edifice. We infer that this signal was elastically recovered by a similar pattern of subsidence during the eruption itself. Any dikes that fed the eruption from this source depth would have been hard to detect because of InSAR decorrelation on the edifice, unless they had an opening significantly larger than 1 m.

Villarrica: Post-eruptive uplift following the March 3 2015 eruption from a depth of ~4.2 km and offset from the summit by 5 km to the SE. As at Llaima, deformation on the edifice itself is difficult to measure with available InSAR.

Calbuco: Subsidence during the April 22-23 2015 eruptions from a source at a depth of 8-11 km below the summit.

2. The lack of ground deformation before the March 3 2015 Villarrica eruption, before the Calbuco eruption on April 22-23 2015, and during the April 30 2015 Calbuco eruptions is constrained by observations within about 4, 1 and 4 days of the start of the events. During the 2008-2009 Llaima eruptions the temporal sampling is not as good, and

deformation could have been aliased. Co-eruptive deformation was only detected during the VEI 4 Calbuco eruption while for the rest of the eruptions (VEI 1-2 for Villarrica and Llaima) the potential ground deformation signals are likely ~ 1 order of magnitude smaller than the amplitude of the average atmospheric phase delays, and are not likely to be imaged near the volcano summit that are systematically decorrelated in the available InSAR data. To properly assess the relation of ground deformation and eruption more frequent InSAR sampling is needed with high-resolution topographic data, including measurements closer to the conduit than are routinely available for these three volcanoes.

3. To date, observations from InSAR in the SAVZ have not been ideal for detecting ground deformation or separating real deformation from tropospheric changes. In order to assess these persistent atmospheric signals we recommend SAR data with beams that cover several volcanic edifices and not small swaths as those from spotlight modes. We also recommend observations at these volcanoes during every satellite overflight even in the austral winter to mitigate systematic temporal decorrelation.

Acknowledgements

We acknowledge the CEOS volcano pilot project managed by Simona Zoffoli (ASI) and Michael Poland (USGS) for coordinating data distribution among multiple space agencies. ERS-2, ENVISAT and Sentinel-1A data were provided by the European Space Agency. ALOS and ALOS-2 data were provided by the Japanese Aerospace Exploration Agency through the Alaska Satellite Facility (ASF), NASA and UNAVCO. COSMO-SkyMED data were provided by Agenzia Spaziale Italiana (ASI). RADARSAT-2 data were provided by the Canadian Space Agency (CSA); MacDonald, Dettwiler & Associates (MDA) Ltd.; and the SOAR and CSA-SOAR-ASI programs. TerraSAR-X data were provided of Deutsches Zentrum für Luft- und Raumfahrt (DLR). UAVSAR data courtesy of NASA/JPL-Caltech. M.E.P. and F.D. were partly supported by NASA grants NNX16AK87G, NNX12AO31G, NNX12AM24G issued through the Science Mission Directorate's Earth Science Division. F.D. acknowledges CONICYT-Becas Chile and the NASA ESSF program for PhD fellowships. We thank Caroline Bouvet de Maisonneuve (Earth Observatory of Singapore), Jacqueline Salzer (GFZ Potsdam),

Michael Poland (USGS), Charles Wicks (USGS), Paul Lundgren (JPL), Andrés Rivera (CECS, Chile), Daniel Bertin, Loreto Córdova, and José Naranjo (SERNAGEOMIN) for sharing unpublished data and discussions. We also thank Piyush Agram and Eric Fielding (JPL) for their help with the ISCE software and for providing prototype additions for processing RS2 zero-doppler data. The GMT software (Wessel and Smith, 1998) was used to create several figures. We acknowledge editor Jürgen Neuberg, Falk Amelung and an anonymous reviewer for their thorough reviews that improved the quality of this work.

Figure Captions

Figure 1. Location map of Llaima, Villarrica and Calbuco volcanoes (red triangles) over the shaded SRTM topography with the footprint of all the analyzed SAR frames. The ERS-2 swath is the same as ENVISAT track 239. Black triangles are Holocene volcanoes (Siebert et al., 2010). Dashed and solid black lines show the extent of the ENVISAT extended and nominal mission frames respectively. TSX swaths are shown for reference as we only processed a few interferograms (**Table 1**). Inset shows the location of the southern Andes within South America. The lower box shows the time span of the processed data sets for each platform as well as the different eruptions (purple dashed lines).

Figure 2. Satellite false color images from (a) after the start of the Llaima April 3 2009 eruption which shows lava effusion over the summit glacier, and (b) after the start of the Villarrica March 3 2015 eruption which shows the active lava lake and tephra that covers the summit glacier. Images from NASA EO-1 ALI instrument, EO1A2330872009098110PF_1T (09/04/08), and EO1A2330872015064110KF (15/03/09), band combinations R10 G6 B4. Grid units are km in UTM coordinates, WGS84 datum, zone 19S. Color scales have been equalized to highlight the lava flows and the lava lake.

Figure 3. Interferogram time series from ALOS at Llaima spanning January 2007-February 2011 showing the mean line of sight ground velocities from two different satellite paths. a) Path 117 mean velocity, no empirical correction for atmospheric signal

correlated with topography. **b)** Path 116 mean velocity, also no empirical correction. **c)** Path 117 mean velocity with empirical correction. **d)** Path 116 mean velocity with empirical correction. The masked square in **a** to **d** east of Llaima is the area where Fournier et al., [2010] detected a possible flank instability signal, which has been masked out for the time series as it has unwrapping errors and is a localized signal that is not of interest in our search for edifice-scale deformation. The black circles in figures **a** to **d** are the location of the deformation profiles shown in **e** to **h**, the black arrow is the flight direction and the grey arrow is the look direction with the incidence angle. **e, f, g, h)** Deformation time series for **a, b, c,** and **d**, respectively. In **e** to **h**, the vertical red bars are the January 1 2008 and April 3 2009 Llaima eruptions. The yellow circle in **e** to **h** shows the outlier in the time series interpreted as pre eruptive deformation before the April 3 2009 eruption (**Figure 5**). We do not think that the rest of the points in the deformation time series (**a, b, c,** and **d**) indicate real deformation because the rates are not consistent between the two paths and previous work has found ALOS time series uncertainties are ~ 2.5 cm/yr (e.g., Philibosian and Simons (2011); Ebmeier et al. (2013)).

Figure 4. Interferograms spanning the January 1 2008 and April 3 2009 eruptions at Llaima showing wrapped line of sight ground displacements. **a, b, c, d** and **e)** ENVISAT track 304 ascending interferograms, **f, g)** ENVISAT track 10 descending interferograms, **h)** ENVISAT track 239 descending interferogram. Red triangles are Llaima northern and southern summits. Horizontal bars beneath the interferograms show the time covered by each one. Red line is the January 1 2008 eruption. The fringes around the volcano are most likely produced by topography correlated atmospheric phase signals, while the black box in **b** and **c** shows a signal possibly produced by flank instability (Fournier et al., 2010). The latter signal is not evident in the rest of the interferograms due to decorrelation. The track 239 interferogram does not show ground deformation, most likely due to zero cumulative ground deformation during the covered time span – since inflation was observed before the eruption (**Figure 5**) this implies that any subsidence must have been equal and opposite of the inflation within measurement error.

Figure 5. Llaima interferograms (**a, d**), model prediction (**b, e**) and residual between data and model (**c, f**) of the presumed ground deformation from a sill intrusion (model

parameters in **Table 3**) before the April 3 2009 eruption. See **Figure 3** for these interferograms compared to the rest of the time series. The black lines are the surface projection of the inferred sill and the thick black line is the sill top. Red triangles are the north and south Llaima summits. The box in **a** to **f** east of Llaima with no data is the area where Fournier et al. (2010) detected a possible flank instability signal (**Figure 4**), and has been masked in radar coordinates as it has unwrapping errors and deformation from the sill is not visible in the region.

Figure 6. a-b) Mean ground velocities at Villarrica spanning the March 03 2015 eruption from CSK (**a**) and S1A (**b**) that show different velocities over a common time period in areas of high relief and so are interpreted to represent atmospheric effects and not real ground deformation. Time series uncertainties are ± 1.6 and 2.2 cm/yr for S1A and CSK respectively. Thin black and blue lines are the 2011 glacier limits and the debris covered glacier (Rivera et al., 2015). Blue and red lines are caldera 1-2 and caldera 3 rims from (Moreno and Clavero, 2006). Red triangle shows volcanoes summit. Black and grey arrows are the satellite heading and line of sight direction. Blue and black squares are OVDAS continuous GPS and tiltmeters respectively and are shown for comparison. **c)** Deformation time series for (**a**) and (**b**) (red and blue respectively). Pixels error bars were calculated from the variance of each interferogram in non-deforming areas under the assumption that the phase delays are spatially uncorrelated. Time series were not corrected for topography correlated phase delays because the small swath of the CSK data does not include enough high relief areas for a reliable correction. Red line shows the time of the March 3 2015 eruption.

Figure 7. Interferograms at Villarrica (**a, d, g**), model prediction (**b, e, h**) and residual (**c, f, i**) of what we think is real ground deformation after the March 3 2015 eruption using a Mogi source southeast of the summit (model parameters in **Table 5**). Blue and black squares are OVDAS continuous GPS and tilt meters respectively and are shown for comparison. Black point is the location of the Mogi source. Black dashed lines are the swath of TSX spotlight data that have been acquired which do not completely cover the observed deformation signal. Other labels are the same as **Figure 6**.

Figure 8. Calbuco Sentinel-1 interferograms showing ground deformation from the April 22-23 2015 eruptions (**a, d, g, j**), model predictions (**b, e, h, k**) and residuals (**c, f, i, l**) with results for the joint inversions for spherical (**a-f**) and spheroidal (**g-l**) point sources. Purple square circle shows the location of the OVDAS tilt meter. Red circle shows the location of the best-fit sources (model parameters given in **Table 1**).

Figure 9. Examples of 1-day CSK and 2-days UAVSAR interferograms covering Villarrica volcano. The season, repeat period and acquisition dates are labeled. All the interferograms are wrapped and only **a** and **b** were filtered. Blue and black squares are OVDAS continuous GPS and tilt meters respectively and are shown for comparison. Dashed black lines are the swath of TSX spotlight data (Supplementary material). Other labels are as in **Figure 6**. The fringes near the caldera rim in **a** and within the glacier outlines in **c** and **d** are produced by both glacier changes and DEM errors.

Tables

Table 1. List of all the processed InSAR data for the different volcanoes studied. The number of synthetic aperture radar (SAR) images analyzed and the number of interferograms used in time series are in the column labeled as “SAR” and “TS”. UAVSAR NW-SE pass means that the aircraft flew on a NW-SE direction.

Volcano	Satellite	Wavelength (cm)	Dates (yy/mm/dd)	Track	Pass	Beam mode	SAR	Ints	TS
Llaima/Villarrica	ERS-2	5.6	97/10/23-00/12/21	239	D	----	6	6	---
Llaima/Villarrica	ENVISAT	5.6	02/12/10-08/11/18	10	D	IS2	26	135	---
Llaima/Villarrica	ENVISAT	5.6	02/12/26-09/04/23	239	D	IS2	24	142	---
Llaima/Villarrica	ENVISAT	5.6	03/02/04-10/04/13	304	A	IS2	31	186	---
Llaima/Villarrica	ALOS	23.6	06/12/04-11/03/17	117	A	FBD, FBS	16	92	22
Llaima/Villarrica	RS2	5.5	12/12/21-15/03/17	---	D	Wide Fine 2	10	43	---
Llaima/Villarrica	Sentinel-1A	5.5	14/10/23-15/06/08	83	D	IW	9	11	10
Llaima/Villarrica	Sentinel-1A	5.5	15/01/08-15/06/01	164	A	IW	6	8	---
Llaima/Villarrica	Sentinel-1A	5.5	14/10/11-15/05/27	91	A	IW	10	15	---
Llaima/Villarrica	ALOS-2	24.2	15/02/21-15/05/16	129	D	WD1	3	3	---
Llaima	ALOS	23.6	10/02/24-11/01/12	419	D	FBS	2	2	---
Llaima	ALOS	23.6	07/02/17-11/02/28	116	A	FBD, FBS	18	104	27
Llaima	ENVISAT	5.6	10/11/01-12/03/25	61	A	IS6	18	75	25
Llaima	CSK	3.1	11/07/18-11/07/19	---	D	HIMAGE	2	1	---
Llaima	CSK	3.1	11/12/26-14/05/23	---	D	HIMAGE	25	56	---
Llaima	UAVSAR	23.8	13/03/25-15/03/28	---	SE-NW	PolSAR	3	3	---
Llaima	UAVSAR	23.8	13/03/27-15/03/30	---	D	PolSAR	3	3	---
Villarrica	ALOS	23.6	08/01/15-11/01/12	419	D	FBS	3	3	---
Villarrica	ALOS	23.6	07/02/05-11/02/16	118	A	FBD, FBS	17	87	27
Villarrica	ENVISAT	5.6	10/12/20-12/03/14	334	A	IS6	12	37	---
Villarrica	CSK	3.1	11/07/18-11/07/19	---	D	HIMAGE	2	1	---
Villarrica	CSK	3.1	12/03/14-12/03/15	---	D	HIMAGE	2	1	---
Villarrica	CSK	3.1	14/06/16-14/09/20	---	D	HIMAGE	11	15	---

Villarrica	CSK	3.1	14/12/01-15/05/26	---	D	HIMAGE	31	66	15
Villarrica	UAVSAR	23.8	13/03/25-15/03/20	---	NW-SE	PolSAR	6	8	---
Villarrica	UAVSAR	23.8	13/03/25-15/03/30	---	D	PolSAR	3	3	---
Villarrica	UAVSAR	23.8	13/03/27-15/03/30	---	A	PolSAR	4	6	---
Villarrica	TSX	3.1	15/03/23-15/05/06	13	A	Spotlight	4	4	---
Calbuco	ENVISAT	5.6	03/06/19-05/09/01	239	D	IS2	7	7	---
Calbuco	ENVISAT	5.6	03/03/25-05/09/20	10	D	IS2	8	10	---
Calbuco	ENVISAT	5.6	04/01/04-10/03/28	75	A	IS2	5	2	---
Calbuco	ALOS	23.6	07/04/26-11/02/04	120	A	FBD, FBS	13	78	17
Calbuco	ENVISAT	5.6	10/11/28-12/03/22	18	A	IS6	17	70	25
Calbuco	RS2	5.5	12/12/21-15/05/28	---	D	Wide Fine 2	15	91	---
Calbuco	UAVSAR	23.8	13/03/27-15/03/30	---	A	PolSAR	3	3	---
Calbuco	UAVSAR	23.8	13/03/27-15/03/30	---	D	PolSAR	3	3	---
Calbuco	Sentinel-1A	5.5	15/02/25-15/06/25	164	A	IW	9	8	---
Calbuco	Sentinel-1A	5.5	14/11/02-15/05/01	62	A	IW	7	9	---
Calbuco	Sentinel-1A	5.5	14/10/23-15/06/08	83	D	IW	12	20	11
Calbuco	ALOS-2	24.2	15/03/04-15/04/29	36	A	SM3	2	1	---
Calbuco	ALOS-2	24.2	15/02/21-15/05/16	129	D	WD1	3	3	---
Calbuco	CSK	3.1	15/04/23-15/04/24	---	D	HIMAGE	2	1	---
Calbuco	CSK	3.1	15/04/24-15/04/25	---	D	HIMAGE	2	1	---
Calbuco	CSK	3.1	15/04/29-15/05/31	---	D	HIMAGE	7	4	---
Total							422	1427	

Table 2. Llaima ALOS ascending interferograms used in the joint inversion for the inflation before the April 3 2009 eruption. B_{perp} is the perpendicular baseline in meters. RMS is the root mean square of the residual after the synthetic interferogram predicted by the best fit model has been subtracted from the data.

ALOS Path	Master – slave images (yy/mm/dd)	Sill opening (m)	RMS	B_{perp}
116	09/02/22 - 07/02/17	0.27	1.59	-861
116	09/02/22 - 07/04/04	0.20	1.08	-1452
117	09/03/11 - 07/03/06	0.14	0.71	-1089

Table 3. Llaima best fit sill model with error bounds. X_s centroid EW coordinate, Y_s centroid NS coordinate, Z_s centroid depth, θ strike, δ dip, L length, W width, U opening. Sill centroid position in WGS84 UTM 19S datum.

X_s (km)	Y_s (km)	Z_s (km)	θ (°)	δ (°)	L (km)	W (km)	U (cm)
259.9 ± 0.2	5710.8 ± 0.2	5.2 ± 0.6	354 ± 10	16 ± 4	9.8 ± 1.1	6.8 ± 0.8	14 ± 11

Table 4. Villarrica CSK descending interferograms used in the joint inversion for the inflation event after the March 3 2015 eruption. RMS and B_{perp} as in **Table 2** with ΔV is the inverted volumetric variation.

Master – slave images (yy/mm/dd)	ΔV (km ³)	RMS (cm)	B_{perp}
15/04/12 - 15/02/11	0.006	0.56	29
15/04/12 - 15/02/23	0.0073	0.46	133
15/04/12 - 15/03/11	0.0057	0.45	-88
15/05/10 - 15/02/19	0.0069	0.37	-14
15/05/14 - 15/02/19	0.0075	0.39	-36
15/05/14 - 15/03/27	0.0097	0.42	153

Table 5. Villarrica best fit Mogi source model for the inflation after the March 3 2015 eruption with error bounds. X_s source EW coordinate, Y_s source NS coordinate, Z_s source depth beneath sea level. Mogi centroid coordinates in WGS84 UTM 19S datum.

X_s (km)	Y_s (km)	Z_s (km)
251.0 ± 0.03	5629.6 ± 0.04	4.2 ± 0.1

Table 6. Calbuco S1A interferograms used in the joint inversion for the deflation signal during the April 22-23 2015 eruptions. RMS and B_{perp} as in **Table 2**. The spheroid source strength is the adimensional pressure to shear modulus ratio.

Source	Master - slave images (yy/mm/dd)	Source strength	RMS (cm)	B_{perp}
Sphere	15/04/26 - 15/04/14	0.055 km^3	0.85	-44
Sphere	15/05/03 - 15/03/23	0.035 km^3	0.74	-20
Spheroid	15/04/26 - 15/04/14	0.0733	0.80	-44
Spheroid	15/05/03 - 15/03/23	0.0771	0.66	-20

Table 7. Calbuco best fit source models. We fixed the spheroid semi-major axis, otherwise the inversion predicts an unrealistic large source (Pritchard and Simons, 2004). X_s centroid EW coordinate, Y_s centroid NS coordinate, Z_s centroid depth, a major semi axis, b minor semi axis. Centroid coordinates are in WGS84 UTM 18S datum.

Model	X_s (km)	Y_s (km)	Z_s (km)	a (km)	b (km)	Plunge (°)	Trend (°)
Spheroid	699.2 ± 0.2	5419.0 ± 0.3	7.78 ± 0.3	1 (fixed)	0.42 ± 0.04	77 ± 2	293 ± 7
Sphere	696.3 ± 0.3	5419.4 ± 0.2	10.7 ± 0.4	---	---	---	---

Table 8. Summary of InSAR temporal coherence loss. We did not assess the coherence loss of ERS-2, Sentinel-1A, ALOS-2 and TerraSAR-X data due to the small data sets we processed. ⁽¹⁾ Equivalent to 2-3 repeat periods. ⁽²⁾ ALOS interferograms calculated with a winter scene and scenes from other seasons are coherent. ⁽³⁾ Not analyzed because of the satellite drifting orbit. ⁽⁴⁾ Not analyzed due to the small data set. ⁽⁵⁾ ALOS interferograms with temporal baselines longer than 3 years are not coherent due to geometrical rather than temporal decorrelation.

Satellite	Repeat period (days)	Beam	Polarization	Maximum temporal baseline to sustain coherence in lava flows and forests		Maximum temporal baseline to sustain coherence only in lava flows
				Summer	Winter	
ENVISAT	35	IS2	VV	2 months ⁽¹⁾	<35 days	> 4 years

ENVISAT	30	IS6	HH	2-3 months ⁽¹⁾	< 35 days	Not analyzed ⁽³⁾
RADARSAT-2	24	Wide Fine 2	HH	1.5 – 2.5 months ⁽¹⁾	24 days	Not analyzed ⁽⁴⁾
ALOS	46	FBS	HH	> 3 years	< 46 days ⁽²⁾	3 years ⁽⁵⁾
CSK	1-16	HIMAGE	HH	1 month	12 days	Not analyzed ⁽⁴⁾

Table 9. Summary of InSAR temporal coherence loss on top of the glacier covered summits of Llaima and Villarrica. ⁽¹⁾ Only 2-day pairs were available for the analysis.

Satellite	Beam	Polarization	Maximum temporal baseline to sustain coherence on Llaima and Villarrica summits
ERS-2	--	VV	< 35 days
ENVISAT	IS2	VV	< 35 days
ENVISAT	IS6	HH	< 30 days
ALOS	FBS	HH	< 46 days
RADARSAT-2	Wide Fine 2	HH	< 24 days
CSK	HIMAGE	HH	1 day
Sentinel-1A	IW	VV	< 12 days
TSX	Spotlight	HH	< 11 days
ALOS-2	WD1	HH/HV	< 42 days
UAVSAR	PolSAR	HH	2 days ⁽¹⁾

References

Uncategorized References

- Acocella, V., Di Lorenzo, R., Newhall, C. and Scandone, R., 2015. An overview of recent (1988 to 2014) caldera unrest: Knowledge and perspectives. *Reviews of Geophysics*, 53(3): 896-955.10.1002/2015rg000492.
- Albino, F., Pinel, V., Massol, H. and Collombet, M., 2011. Conditions for detection of ground deformation induced by conduit flow and evolution. *Journal of Geophysical Research-Solid Earth*, 116.10.1029/2010jb007871.
- Amoruso, A. and Crescentini, L., 2009. Shape and volume change of pressurized ellipsoidal cavities from deformation and seismic data. *Journal of Geophysical Research-Solid Earth*, 114.10.1029/2008jb005946.
- Anderson, K.R. and Poland, M.P., 2016. Bayesian estimation of magma supply, storage, and eruption rates using a multiphysical volcano model: Kīlauea Volcano, 2000–2012. *Earth and Planetary Science Letters*, 447: 161–171.10.1016/j.epsl.2016.04.029.
- Baker, S. and Amelung, F., 2012. Top-down inflation and deflation at the summit of Kīlauea Volcano, Hawai'i observed with InSAR. *Journal of Geophysical Research-Solid Earth*, 117.10.1029/2011jb009123.

- Basualto, D., Moreno, H., Peña, P., Muñoz, J., Delgado, C. and Gallegos, C., 2009, Actividad sísmica del actual ciclo eruptivo del volcán Llaima, periodo enero 2005-febrero 2008, XII Congreso Geológico Chileno, S7_006.
- Bathke, H., Shirzaei, M. and Walter, T.R., 2011. Inflation and deflation at the steep-sided Llaima stratovolcano (Chile) detected by using InSAR. *Geophysical Research Letters*, 38.10.1029/2011gl047168.
- Beauducel, F., Briole, P. and Froger, J.L., 2000. Volcano-wide fringes in ERS synthetic aperture radar interferograms of Etna (1992-1998): Deformation or tropospheric effect? *Journal of Geophysical Research-Solid Earth*, 105(B7): 16391-16402.10.1029/2000jb900095.
- Bekaert, D.P.S., Hooper, A. and Wright, T.J., 2015. A spatially variable power law tropospheric correction technique for InSAR data. *Journal of Geophysical Research-Solid Earth*, 120(2): 1345-1356.10.1002/2014jb011558.
- Berardino, P., Fornaro, G., Lanari, R. and Sansosti, E., 2002. A new algorithm for surface deformation monitoring based on small baseline differential SAR interferograms. *Ieee Transactions on Geoscience and Remote Sensing*, 40(11): 2375-2383.10.1109/tgrs.2002.803792.
- Bertin, D., Amigo, A. and Bertin, L., 2015, Erupción del volcán Villarrica 2015: Productos emitidos y volumen involucrado, XIV Congreso Geológico Chileno, III, 249-252.
- Biggs, J., Ebmeier, S.K., Aspinall, W.P., Lu, Z., Pritchard, M.E., Sparks, R.S.J. and Mather, T.A., 2014. Global link between deformation and volcanic eruption quantified by satellite imagery. *Nature Communications*, 5.10.1038/ncomms4471.
- Bouvet de Maisonneuve, C., 2011. Petrologic and numerical modeling study of strombolian eruption dynamics at Volcán Llaima (Chile). PhD Thesis, University de Geneve, Geneve, 158 pp.
- Bouvet de Maisonneuve, C., Dungan, M.A., Bachmann, O. and Burgisser, A., 2012. Insights into shallow magma storage and crystallization at Volcan Llaima (Andean Southern Volcanic Zone, Chile). *Journal of Volcanology and Geothermal Research*, 211: 76-91.10.1016/j.jvolgeores.2011.09.010.
- Bouvet de Maisonneuve, C., Dungan, M.A., Bachmann, O. and Burgisser, A., 2013. Petrological Insights into Shifts in Eruptive Styles at Volcan Llaima (Chile). *Journal of Petrology*, 54(2): 393-420.10.1093/petrology/egs073.
- Bredemeyer, S. and Hansteen, T.H., 2014. Synchronous degassing patterns of the neighbouring volcanoes Llaima and Villarrica in south-central Chile: the influence of tidal forces. *International Journal of Earth Sciences*, 103(7): 1999-2012.10.1007/s00531-014-1029-2.
- Casertano, L., 1963a. Actividad del volcán Villarrica en el curso de este siglo. *Universidad de Chile, Boletín*, 41: 48-54
- Casertano, L., 1963b. Actividad del volcán Villarrica en el curso de este siglo. *Universidad de Chile, Boletín*, 40: 22-28
- Castruccio, A., Clavero, J., Segura, A., Samaniego, P., Roche, O., Le Penne, J.-L. and Droguett, B., 2016. Eruptive parameters and dynamics of the April 2015 sub-Plinian eruptions of Calbuco volcano. *Bulletin of Volcanology*, 78(62).10.1007/s00445-016-1058-8.
- Cembrano, J. and Lara, L., 2009. The link between volcanism and tectonics in the southern volcanic zone of the Chilean Andes: A review. *Tectonophysics*, 471(1-2): 96-113.10.1016/j.tecto.2009.02.038.

- Chaussard, E. and Amelung, F., 2012. Precursory inflation of shallow magma reservoirs at west Sunda volcanoes detected by InSAR. *Geophysical Research Letters*, 39.10.1029/2012gl053817.
- Chaussard, E., Amelung, F. and Aoki, Y., 2013. Characterization of open and closed volcanic systems in Indonesia and Mexico using InSAR time series. *Journal of Geophysical Research-Solid Earth*, 118(8): 3957-3969.10.1002/jgrb.50288.
- Córdova, L., Alarcón, A., Mardones, C., Cardona, C., Gil, F., Rojas, G., Quijada, J., Le Mével, H., Feigl, K., DeMets, C. and Lundgren, P., 2015. Monitoreo de la deformación en volcanes chilenos mediante técnica GPS, resultados asociados a la actividad de los volcanes Laguna del Maule, Copahue y Villarrica., XIV Congreso Geológico Chileno, III, 233-236.
- Currenti, G., Napoli, R. and Del Negro, C., 2011. Toward a realistic deformation model of the 2008 magmatic intrusion at Etna from combined DInSAR and GPS observations. *Earth and Planetary Science Letters*, 312(1-2): 22-27.10.1016/j.epsl.2011.09.058.
- Delgado, F., Pritchard, M., Lohman, R. and Naranjo, J.A., 2014. The 2011 Hudson volcano eruption (Southern Andes, Chile): Pre-eruptive inflation and hotspots observed with InSAR and thermal imagery. *Bulletin of Volcanology*, 76(5): 19.10.1007/s00445-014-0815-9.
- Delgado, F., Pritchard, M.E., Basualto, D., Lazo, J., Cordova, L. and Lara, L.E., 2016. Rapid reinflation following the 2011-2012 rhyodacite eruption at Cordon Caulle volcano (Southern Andes) imaged by InSAR: Evidence for magma reservoir refill. *Geophysical Research Letters*, 43(18): 9552-9562.10.1002/2016gl070066.
- Doin, M.P., Lasserre, C., Peltzer, G., Cavalie, O. and Doubre, C., 2009. Corrections of stratified tropospheric delays in SAR interferometry: Validation with global atmospheric models. *Journal of Applied Geophysics*, 69(1): 35-50.10.1016/j.jappgeo.2009.03.010.
- Dvorak, J.J. and Dzurisin, D., 1997. Volcano geodesy: The search for magma reservoirs and the formation of eruptive vents. *Reviews of Geophysics*, 35(3): 343-384.10.1029/97rg00070.
- Dzierma, Y. and Wehrmann, H., 2010. Statistical eruption forecast for the Chilean Southern Volcanic Zone: typical probabilities of volcanic eruptions as baseline for possibly enhanced activity following the large 2010 Concepcion earthquake. *Natural Hazards and Earth System Sciences*, 10(10): 2093-2108.10.5194/nhess-10-2093-2010.
- Dzierma, Y. and Wehrmann, H., 2012. On the likelihood of future eruptions in the Chilean Southern Volcanic Zone: interpreting the past century's eruption record based on statistical analyses. *Andean Geology*, 39(3): 380-393.10.5027/andgeoV39n3-a02.
- Dzurisin, D., 2003. A comprehensive approach to monitoring volcano deformation as a window on the eruption cycle. *Reviews of Geophysics*, 41(1).10.1029/2001rg000107.
- Dzurisin, D. and Lu, Z., 2006. Interferometric synthetic-aperture radar (InSAR). In: D. Dzurisin (Editor), *Volcano Deformation: Geodetic Monitoring Techniques*. Springer, pp. 153-194.
- Ebmeier, S.K., Biggs, J., Mather, T.A. and Amelung, F., 2013. On the lack of InSAR observations of magmatic deformation at Central American volcanoes. *Journal of Geophysical Research-Solid Earth*, 118(5): 2571-2585.10.1002/jgrb.50195.
- Feigl, K.L., Le Mével, H., Ali, S.T., Cordova, L., Andersen, N.L., DeMets, C. and Singer, B.S., 2014. Rapid uplift in Laguna del Maule volcanic field of the Andean Southern Volcanic zone (Chile) 2007-2012. *Geophysical Journal International*, 196(2): 885-901.10.1093/gji/ggt438.

- Fournier, T.J., Pritchard, M.E. and Riddick, S.N., 2010. Duration, magnitude, and frequency of subaerial volcano deformation events: New results from Latin America using InSAR and a global synthesis. *Geochemistry Geophysics Geosystems*, 11: 29.10.1029/2009gc002558.
- Francis, P., Oppenheimer, C. and Stevenson, D., 1993. Endogenous growth of persistently active volcanos. *Nature*, 366(6455): 554-557.10.1038/366554a0.
- Franco, L.E., Palma, J.L., Gil-Cruz, F., Lara, L.E. and San Martin, J.J., 2015, Aspectos sísmológicos relacionados con las erupciones estrombolianas en el último ciclo eruptivo del volcán Llaima, Chile (2007 – 2010), XIV Congreso Geológico Chileno, III, 154-157.
- Froger, J.L., Remy, D., Bonvalot, S. and Legrand, D., 2007. Two scales of inflation at Lastarria-Cordon del Azufre volcanic complex, central Andes, revealed from ASAR-ENVISAT interferometric data. *Earth and Planetary Science Letters*, 255(1-2): 148-163.10.1016/j.epsl.2006.12.012.
- Gurioli, L., Harris, A.J.L., Houghton, B.F., Polacci, M. and Ripepe, M., 2008. Textural and geophysical characterization of explosive basaltic activity at Villarrica volcano. *Journal of Geophysical Research-Solid Earth*, 113(B8).10.1029/2007jb005328.
- Heimisson, E.R., Einarsson, P., Sigmundsson, F. and Brandsdottir, B., 2015. Kilometer-scale Kaiser effect identified in Krafla volcano, Iceland. *Geophysical Research Letters*, 42(19): 7958-7965.10.1002/2015gl065680.
- Henderson, S.T. and Pritchard, M.E., 2013. Decadal volcanic deformation in the Central Andes Volcanic Zone revealed by InSAR time series. *Geochemistry Geophysics Geosystems*, 14(5): 1358-1374.10.1002/ggge.20074.
- Hooper, A., Segall, P. and Zebker, H., 2007. Persistent scatterer interferometric synthetic aperture radar for crustal deformation analysis, with application to Volcan Alcedo, Galapagos. *Journal of Geophysical Research-Solid Earth*, 112(B7).10.1029/2006jb004763.
- Jay, J., Costa, F., Pritchard, M., Lara, L., Singer, B. and Herrin, J., 2014. Locating magma reservoirs using InSAR and petrology before and during the 2011-2012 Cordon Caulle silicic eruption. *Earth and Planetary Science Letters*, 403: 463-463.10.1016/j.epsl.2014.07.021.
- Jolivet, R., Agram, P.S., Lin, N.Y., Simons, M., Doin, M.-P., Peltzer, G. and Li, Z.H., 2014. Improving InSAR geodesy using Global Atmospheric Models. *Journal of Geophysical Research-Solid Earth*, 119(3): 2324-2341.10.1002/2013jb010588.
- Jolivet, R., Grandin, R., Lasserre, C., Doin, M.P. and Peltzer, G., 2011. Systematic InSAR tropospheric phase delay corrections from global meteorological reanalysis data. *Geophysical Research Letters*, 38.10.1029/2011gl048757.
- Kazahaya, K., Shinohara, H. and Saito, G., 1994. Excessive degassing of Izu-Oshima volcano - magma convection in a conduit. *Bulletin of Volcanology*, 56(3): 207-216.10.1007/bf00279605.
- Lara, L.E. and Clavero, J., 2004, Villarrica Volcano (39.5°S), Southern Andes, Chile., Servicio Nacional de Geología y Minería. Boletín. No. 61. 66 p. Santiago.
- Lara, L.E., Orozco, G., Amigo, A. and Silva, C., 2011, Peligros Volcánicos de Chile, Servicio Nacional de Geología y Minería, Carta Geológica de Chile, Serie Geología Ambiental, No.13: 34 p., 1 mapa escala 1:2.000.000. Santiago.

- Lohman, R.B. and Simons, M., 2005. Some thoughts on the use of InSAR data to constrain models of surface deformation: Noise structure and data downsampling. *Geochemistry Geophysics Geosystems*, 6: 12.10.1029/2004gc000841.
- Lu, Z. and Dzurisin, D., 2014. *InSAR Imaging of Aleutian Volcanoes: Monitoring a Volcanic Arc from Space*. Springer-Verlag, Berlin Heidelberg.
- Lundgren, P., Kiryukhin, A., Milillo, P. and Samsonov, S., 2015a. Dike model for the 2012–2013 Tolbachik eruption constrained by satellite radar interferometry observations. *Journal of Volcanology and Geothermal Research*.10.1016/j.jvolgeores.2015.05.011.
- Lundgren, P., Milillo, P., Kiryukhin, A., Samsonov, S., Gil, F., Cordova, M., Tanaka, A. and Owen, S., 2015b, Application of satellite and airborne InSAR to volcano deformation processes in the Pacific Rim, FRINGE Workshop, Eur. Space Agency,
- Masterlark, T., 2007. Magma intrusion and deformation predictions: Sensitivities to the Mogi assumptions. *Journal of Geophysical Research-Solid Earth*, 112(B6).10.1029/2006jb004860.
- Mastin, L.G., Lisowski, M., Roeloffs, E. and Beeler, N., 2009. Improved constraints on the estimated size and volatile content of the Mount St. Helens magma system from the 2004–2008 history of dome growth and deformation. *Geophysical Research Letters*, 36.10.1029/2009gl039863.
- Mastin, L.G., Roeloffs, E., Beeler, N.M. and Quick, J.E., 2008. Constraints on the size, overpressure, and volatile content of the Mount St. Helens magma system from geodetic and dome-growth measurements during the 2004–2006+ eruption. In: D.R. Sherrod, W.E. Scott and P.H. Stauffer (Editors), *A volcano rekindled; the renewed eruption of Mount St. Helens, 2004–2006*. U.S. Geological Survey Professional Paper, pp. 856.
- Mather, T.A., Tsanev, V.I., Pyle, D.M., McGonigle, A.J.S., Oppenheimer, C. and Allen, A.G., 2004. Characterization and evolution of tropospheric plumes from Lascar and Villarrica volcanoes, Chile. *Journal of Geophysical Research-Atmospheres*, 109(D21).10.1029/2004jd004934.
- McTigue, D.F., 1987. Elastic stress and deformation near a finite spherical magma body: Resolution of the point source paradox. *Journal of Geophysical Research: Solid Earth*, 92(B12): 12931–12940.10.1029/JB092iB12p12931.
- Moreno, H., 1993. Volcán Villarrica: Geología y evaluación del riesgo, regiones IX-X, 39°25'S. Informe final., Proyecto Fondecyt, No. 1247, pp. 112.
- Moreno, H. and Clavero, J., 2006, Geología del volcán Villarrica, Regiones de la Araucanía y de los Lagos, Servicio Nacional de Geología y Minería, Carta Geológica de Chile, Serie Geología Básica, No. 98, 35 p., 1 mapa escala 1:50.000.
- Moreno, H., Naranjo, J.A., Peña, P., Muñoz, J., Basualto, D., C., D., Gallegos, C., Dungan, M. and Bouvet de Maisonneuve, C., 2009, El ciclo eruptivo 2007–2009 del volcán Llaima, Andes del sur, XII Congreso Geológico Chileno, S7_018.
- Morgado, E., Parada, M.A., Contreras, C., Castruccio, A., Gutiérrez, F. and McGee, L.E., 2015. Contrasting records from mantle to surface of Holocene lavas of two nearby arc volcanic complexes: Caburgua-Huelemolle Small Eruptive Centers and Villarrica Volcano, Southern Chile. *Journal of Volcanology and Geothermal Research*.1016/j.jvolgeores.2015.09.023.
- Moussallam, Y., Bani, P., Curtis, A., Barnie, T., Moussallam, M., Peters, N., Schipper, C.I., Aiuppa, A., Giudice, G., Amigo, A., Velasquez, G. and Cardona, C., 2016. Sustaining persistent lava lakes:

- Observations from high-resolution gas measurements at Villarrica volcano, Chile. *Earth and Planetary Science Letters*, 454: 237-247.10.1016/j.epsl.2016.09.012.
- Naranjo, J.A., 2015, Nuevo estilo eruptivo del volcán Villarrica: 3 de Marzo 2015., XIV Congreso Geológico Chileno, III, 230-231.
- Naranjo, J.A. and Moreno, H., 2004. Laharic debris-flows from Villarrica Volcano. In: L.E. Lara and J. Clavero (Editors), *Villarrica Volcano (39.5°S), Southern Andes, Chile*. Serv Nac de Geol y Miner, Santiago, pp. 28-38.
- Naranjo, J.A. and Moreno, H., 2005, Geología del volcán Llaima, Región de la Araucanía, Servicio Nacional de Geología y Minería, Carta Geológica de Chile, Serie Geología Básica, No. 88, 33 p., 1 mapa escala 1:50.000, Santiago.
- Naranjo, J.A., Moreno, H., Peña, P., Muñoz, J., Basualto, D., Delgado, C., Gallegos, C., Dungan, M. and Bouvet de Maisonneuve, C., 2009, Estilos eruptivos 2007-2008 del volcán Llaima, Andes del sur, XII Congreso Geológico Chileno, S3_014.
- Nikkhoo, M., Walter, T.R., Lundgren, P.R. and Prats-Iraola, P., 2016. Compound dislocation models (CDMs) for volcano deformation analyses. *Geophysical Journal International*.10.1093/gji/ggw427.
- Okada, Y., 1985. Surface deformation due to shear and tensile faults in a half-space. *Bulletin of the Seismological Society of America*, 75(4): 1135-1154
- Ortiz, A.B. and Zebker, H., 2007. ScanSAR-to-Stripmap mode interferometry processing using ENVISAT/ASAR data. *Ieee Transactions on Geoscience and Remote Sensing*, 45(11): 3468-3480.10.1109/tgrs.2007.895970.
- OVDAS, 2009. Actividad del volcán Llaima, Informes Técnicos No 82 y 85, Región de la Araucanía, Serv Nac Geol Min, Temuco, Chile.
- OVDAS, 2015. Reportes Especiales de Actividad Volcánica, Región de la Araucanía, Año 2015 Marzo 02-18, Serv Nac Geol Min, Temuco, Chile.
- Palma, J.L., Blake, S. and Calder, E.S., 2011. Constraints on the rates of degassing and convection in basaltic open-vent volcanoes. *Geochemistry Geophysics Geosystems*, 12.10.1029/2011gc003715.
- Palma, J.L., Calder, E.S., Basualto, D., Blake, S. and Rothery, D.A., 2008. Correlations between SO₂ flux, seismicity, and outgassing activity at the open vent of Villarrica volcano, Chile. *Journal of Geophysical Research-Solid Earth*, 113(B10).10.1029/2008jb005577.
- Patrick, M.R., Anderson, K.R., Poland, M.P., Orr, T.R. and Swanson, D.A., 2015. Lava lake level as a gauge of magma reservoir pressure and eruptive hazard. *Geology*, 43(9): 831-834.10.1130/g36896.1.
- Pepe, A., Bertran-Ortiz, A., Lundgren, P.R., Rosen, P.A. and Lanari, R., 2011. The stripmap-ScanSAR SBAS approach to fill gaps in stripmap deformation time series with ScanSAR data. *IEEE TRANSACTIONS ON GEOSCIENCE AND REMOTE SENSING*, 49(12): 4788-4804.10.1109/TGRS.2011.2167979.
- Philibosian, B. and Simons, M., 2011. A survey of volcanic deformation on Java using ALOS PALSAR interferometric time series. *Geochemistry Geophysics Geosystems*, 12.10.1029/2011gc003775.
- Pinel, V., Hooper, A., De la Cruz-Reyna, S., Reyes-Davila, G., Doin, M.P. and Bascou, P., 2011. The challenging retrieval of the displacement field from InSAR data for andesitic stratovolcanoes:

- Case study of Popocatepetl and Colima Volcano, Mexico. *Journal of Volcanology and Geothermal Research*, 200(1-2): 49-61.10.1016/j.jvolgeores.2010.12.002.
- Pinel, V., Poland, M.P. and Hooper, A., 2014. Volcanology: Lessons learned from Synthetic Aperture Radar imagery. *Journal of Volcanology and Geothermal Research*, 289: 81-113.10.1016/j.jvolgeores.2014.10.010.
- Poland, M.P. and Lu, Z., 2008. Radar Interferometry Observations of Surface Displacements During Pre- and Coeruptive Periods at Mount St. Helens, Washington, 1992–2005. In: D. Sherrod, W.E. Scott and P.H. Stauffer (Editors), *A Volcano Rekindled: The Renewed Eruption of Mount St. Helens, 2004–2006*, pp. 361-382.
- Poland, M.P., Miklius, A. and Montgomery-Brown, E.K., 2014. Magma supply, storage, and transport at shield-stage Hawaiian volcanoes: Chapter 5 in *Characteristics of Hawaiian volcanoes*. 18015, Reston, VA.
- Pritchard, M.E. and Simons, M., 2004. An InSAR-based survey of volcanic deformation in the central Andes. *Geochemistry Geophysics Geosystems*, 5: 42.10.1029/2003gc000610.
- Remy, D., Bonvalot, S., Briole, P. and Murakami, M., 2003. Accurate measurements of tropospheric effects in volcanic areas from SAR interferometry data: application to Sakurajima volcano (Japan). *Earth and Planetary Science Letters*, 213(3-4): 299-310.10.1016/s0012-821x(03)00331-5.
- Remy, D., Chen, Y., Froger, J.L., Bonvalot, S., Cordoba, L. and Fustos, J., 2015. Revised interpretation of recent InSAR signals observed at Llaima volcano (Chile). *Geophysical Research Letters*, 42(10): 3870-3879.10.1002/2015gl063872.
- Richardson, J.P. and Waite, G.P., 2013. Waveform inversion of shallow repetitive long period events at Villarrica Volcano, Chile. *Journal of Geophysical Research-Solid Earth*, 118(9): 4922-4936.10.1002/jgrb.50354.
- Riel, B., Milillo, P., Simons, M., Lundgren, P., Kanamori, H. and Samsonov, S., 2015. The collapse of Bardarbunga caldera, Iceland. *Geophysical Journal International*, 202(1): 446-453.10.1093/gji/ggv157.
- Rivera, A., Zamora, R., Uribe, J., Wendt, A., Oberreuter, J., Cisternas, S., Gimeno, F. and Clavero, J., 2015. Recent changes in total ice volume on Volcan Villarrica, Southern Chile. *Natural Hazards*, 75(1): 33-55.10.1007/s11069-014-1306-1.
- Romero, J.E., Morgavi, D., Arzilli, F., Daga, R., Caselli, A., Reckziegel, F., Viramonte, J., Díaz-Alvarado, J., Polacci, M., Burton, M. and Perugini, D., 2016. Eruption dynamics of the 22–23 April 2015 Calbuco Volcano (Southern Chile): Analyses of tephra fall deposits. *Journal of Volcanology and Geothermal Research*.10.1016/j.jvolgeores.2016.02.027.
- Rosen, P.A., Hensley, S., Zebker, H.A., Webb, F.H. and Fielding, E.J., 1996. Surface deformation and coherence measurements of Kilauea volcano, Hawaii, from SIR-C radar interferometry. *Journal of Geophysical Research-Planets*, 101(E10): 23109-23125.10.1029/96je01459.
- Ruth, D.C.S. and Calder, E.S., 2014. Plate tephra: Preserved bubble walls from large slug bursts during violent Strombolian eruptions. *Geology*, 42(1): 11-14.10.1130/g34859.1.
- Ruth, D.C.S., Cottrell, E., Cortés, J.A., Kelley, K.A. and Calder, E.S., 2016. From Passive Degassing to Violent Strombolian Eruption: the Case of the 2008 Eruption of Llaima Volcano, Chile. *Journal of Petrology*, 57(9): 1833-1864.10.1093/petrology/egw063.

- Salzer, J., Mehdi, N., Walter, T.R., Sudhaus, H., Reyes-Dávila, G., Bretón, M. and Arambula, R., 2015. Satellite radar data reveal short-term pre-explosive displacements and a complex conduit system at Volcán de Colima, Mexico. *Frontiers in Earth Science*, 2.10.3389/feart.2014.00012.
- Segall, P., 2010. *Earthquake and volcano deformation*. Princeton University Press, Princeton, 432 pp.
- Selles, D. and Moreno, H., 2011, *Geología del volcán Calbuco, Región de Los Lagos, Servicio Nacional de Geología y Minería, Carta Geológica de Chile, Serie Geología Básica 130: 38 p., 1 mapa escala 1:50.000*. Santiago.
- Siebert, L.E.E., Simkin, T.O.M. and Kimberly, P., 2010. *Volcanoes of the World Third Edition*. University of California Press.
- Sigmundsson, F., Hooper, A., Hreinsdottir, S., Vogfjard, K.S., Ofeigsson, B.G., Heimisson, E.R., Dumont, S., Parks, M., Spaans, K., Gudmundsson, G.B., Drouin, V., Arnadottir, T., Jonsdottir, K., Gudmundsson, M.T., Hognadottir, T., Fridriksdottir, H.M., Hensch, M., Einarsson, P., Magnusson, E., Samsonov, S., Brandsdottir, B., White, R.S., Agustsdottir, T., Greenfield, T., Green, R.G., Hjartardottir, A.R., Pedersen, R., Bennett, R.A., Geirsson, H., La Femina, P.C., Bjornsson, H., Palsson, F., Sturkell, E., Bean, C.J., Mollhoff, M., Braiden, A.K. and Eibl, E.P.S., 2015. Segmented lateral dyke growth in a rifting event at Bardarbunga volcanic system, Iceland. *Nature*, 517(7533): 191-U158.10.1038/nature14111.
- Simons, M. and Rosen, P., 2007. Interferometric synthetic aperture radar geodesy. In: T. Herring (Editor), *Treatise on Geophysics 3*. Elsevier, Amsterdam, pp. 391-446.
- Stern, C.R., 2004. Active Andean volcanism: its geologic and tectonic setting. *Revista Geologica De Chile*, 31(2): 161-206
- Stevens, N.F. and Wadge, G., 2004. Towards operational repeat-pass SAR interferometry at active volcanoes. *Natural Hazards*, 33(1): 47-76.10.1023/B:NHAZ.0000035005.45346.2b.
- Valderrama, O., Franco, L. and Gil-Cruz, F., 2015, *Erupción intempestiva del volcán Calbuco, Abril 2015, XIV Congreso Geológico Chileno., III, 91-93*.
- Van Eaton, A.R., Amigo, A., Bertin, D., Mastin, L.G., Giacosa, R.E., Gonzalez, G., Valderrama, O., Fontijn, K. and Behnke, S.A., 2016. Volcanic lightning and plume behavior reveal evolving hazards during the April 2015 eruption of Calbuco volcano, Chile. *Geophysical Research Letters*.10.1002/2016GL068076.
- Velez, M.L., Euillades, P., Blanco, M. and Euillades, L., 2015. Ground Deformation Between 2002 and 2013 from InSAR Observations. In: F. Tassi, O. Vaselli and A.T. Caselli (Editors), *Copahue Volcano. Active Volcanoes of the World*. Springer-Verlag Berlin Heidelberg, pp. 293.
- Walker, G.P.L., 1989. Gravitational (density) controls on volcanism, magma chambers and intrusions. *Australian Journal of Earth Sciences*, 36(2): 149-165.10.1080/08120098908729479.
- Wauthier, C., Cayol, V., Kervyn, F. and d'Oreye, N., 2012. Magma sources involved in the 2002 Nyiragongo eruption, as inferred from an InSAR analysis. *Journal of Geophysical Research-Solid Earth*, 117.10.1029/2011jb008257.
- Wessel, P. and Smith, W.H.F., 1998. New, improved version of generic mapping tools released. *Eos, Transactions American Geophysical Union*, 79(47): 579-579.10.1029/98EO00426.
- Wicks, C., de la Llera, J.C., Lara, L.E. and Lowenstern, J., 2011. The role of dyking and fault control in the rapid onset of eruption at Chaiten volcano, Chile. *Nature*, 478(7369): 374-+.10.1038/nature10541.

- Williams, C.A. and Wadge, G., 1998. The effects of topography on magma chamber deformation models: Application to Mt. Etna and radar interferometry. *Geophysical Research Letters*, 25(10): 1549-1552.10.1029/98GL01136.
- Witter, J.B. and Calder, E.S., 2004. Magma degassing at Villarrica volcano. In: L.E. Lara and J. Clavero (Editors), *Villarrica Volcano (39.5°S), Southern Andes, Chile*. Serv Nac de Geol y Miner, Santiago, pp. 46-52.
- Witter, J.B., Kress, V.C., Delmelle, P. and Stix, J., 2004. Volatile degassing, petrology, and magma dynamics of the Villarrica Lava Lake, Southern Chile. *Journal of Volcanology and Geothermal Research*, 134(4): 303-337.10.1016/j.jvolgeores.2004.03.002.
- Yang, X.M., Davis, P.M. and Dieterich, J.H., 1988. Deformation from inflation of a dipping finite prolate spheroid in an elastic half-space as a model for volcanic stressing. *Journal of Geophysical Research-Solid Earth and Planets*, 93(B5): 4249-4257.10.1029/JB093iB05p04249.
- Zebker, H.A., Amelung, F. and Jonsson, S., 2000. Remote sensing of volcano surface and internal processes using radar interferometry. In: P.J. Mousinis-Mark, J.A. Crisp and J.H. Fink (Editors), *Remote Sensing of Active Volcanism*, Geophysical Monograph Series, vol. 116. American Geophysical Union, Washington D.C., pp. 179-205.

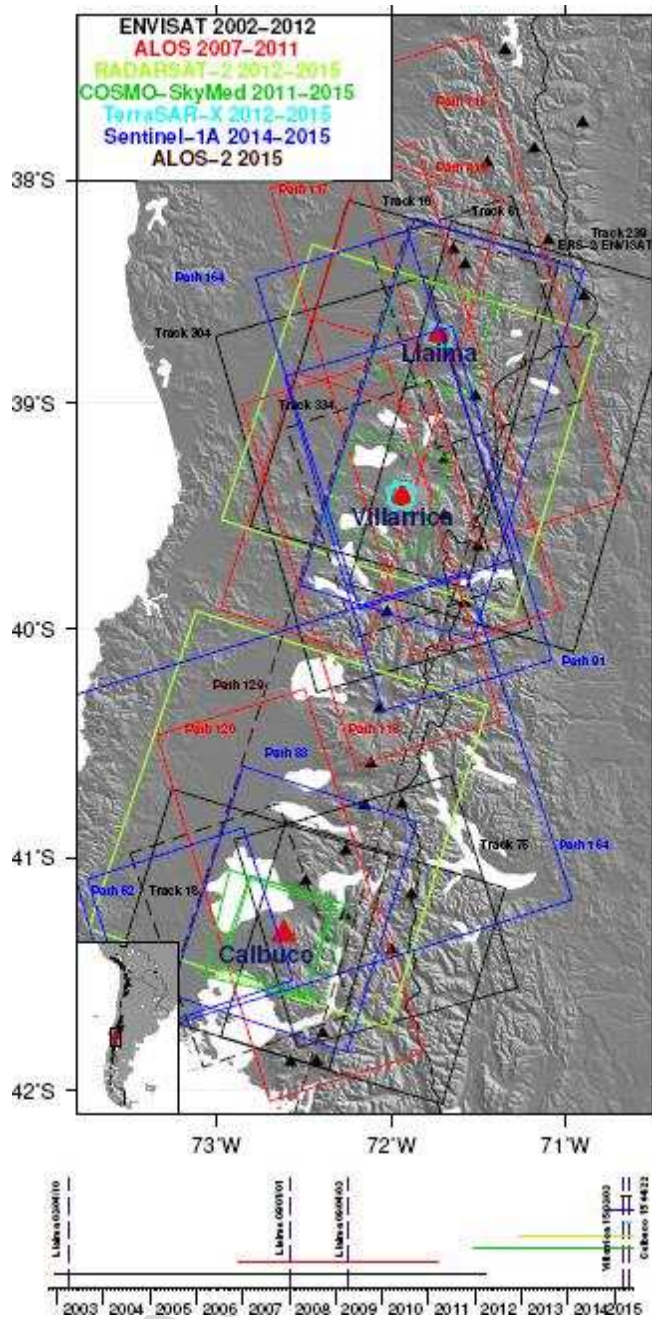


Fig. 1

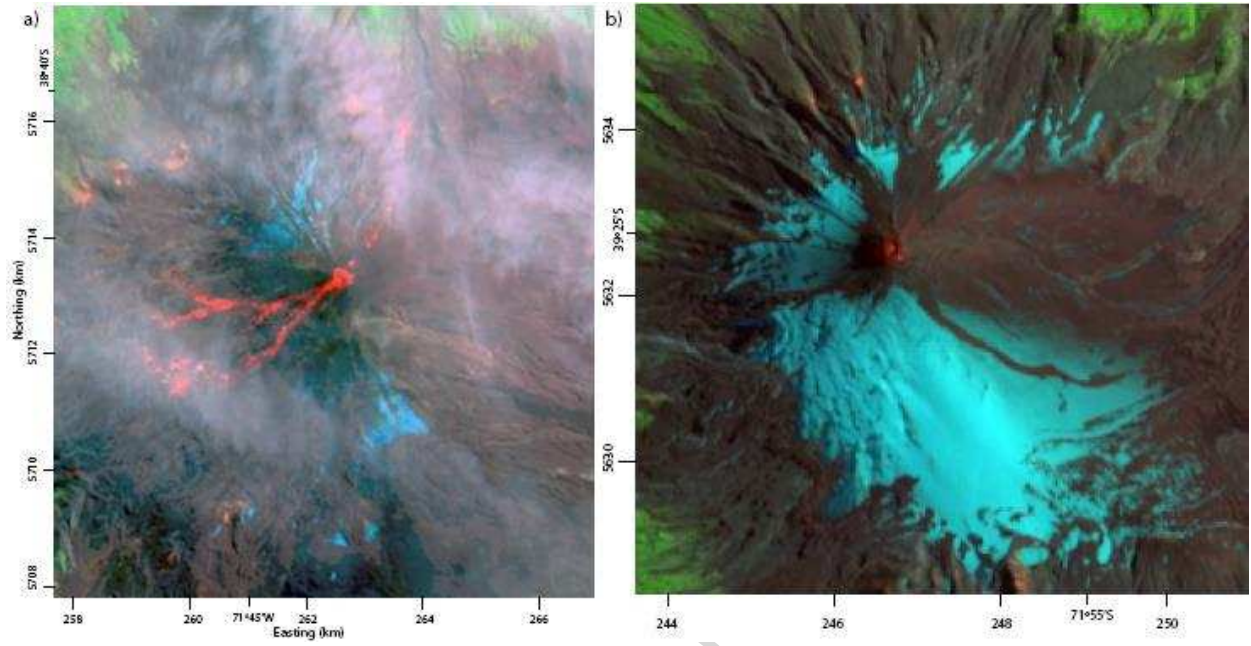


Fig. 2

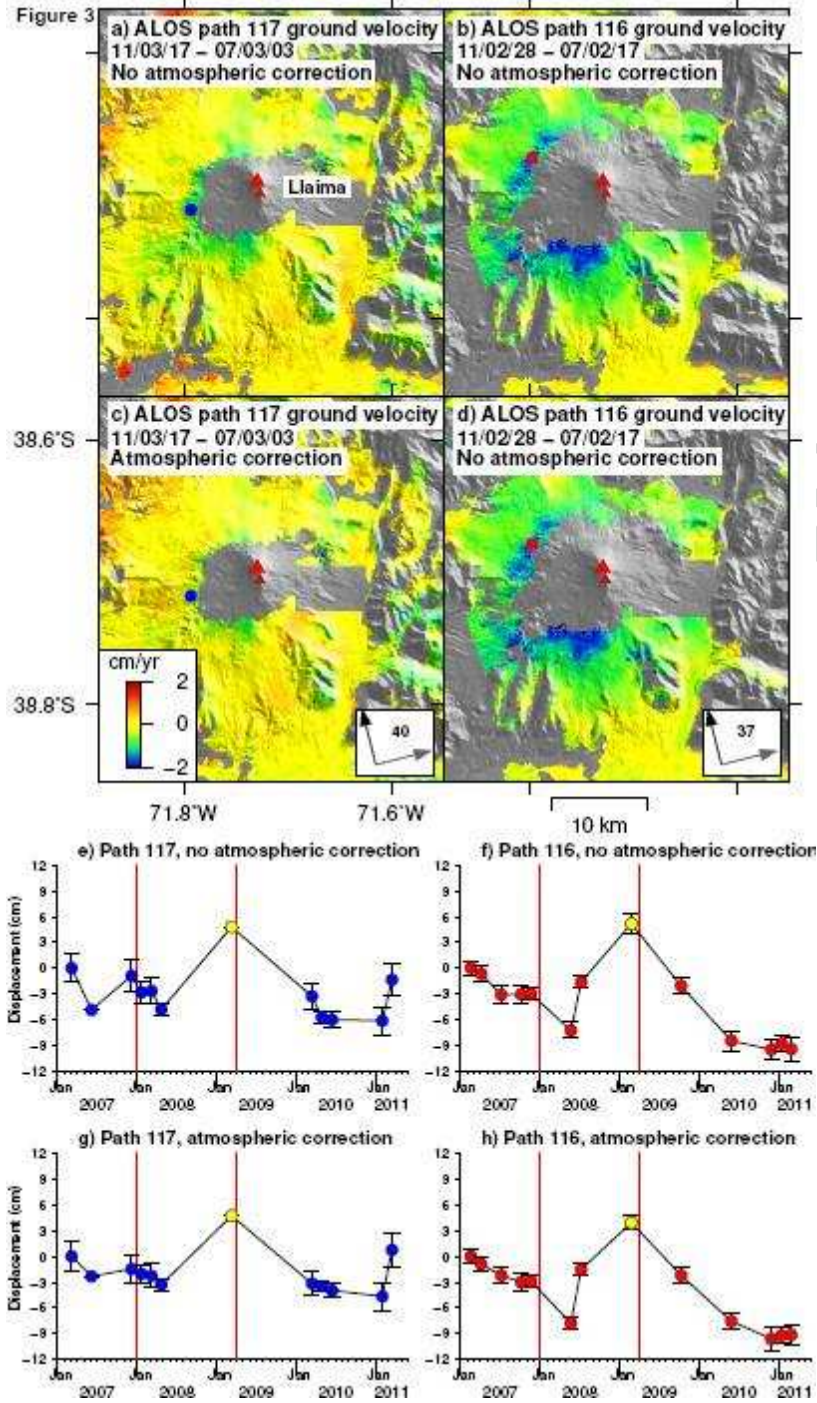


Fig. 3

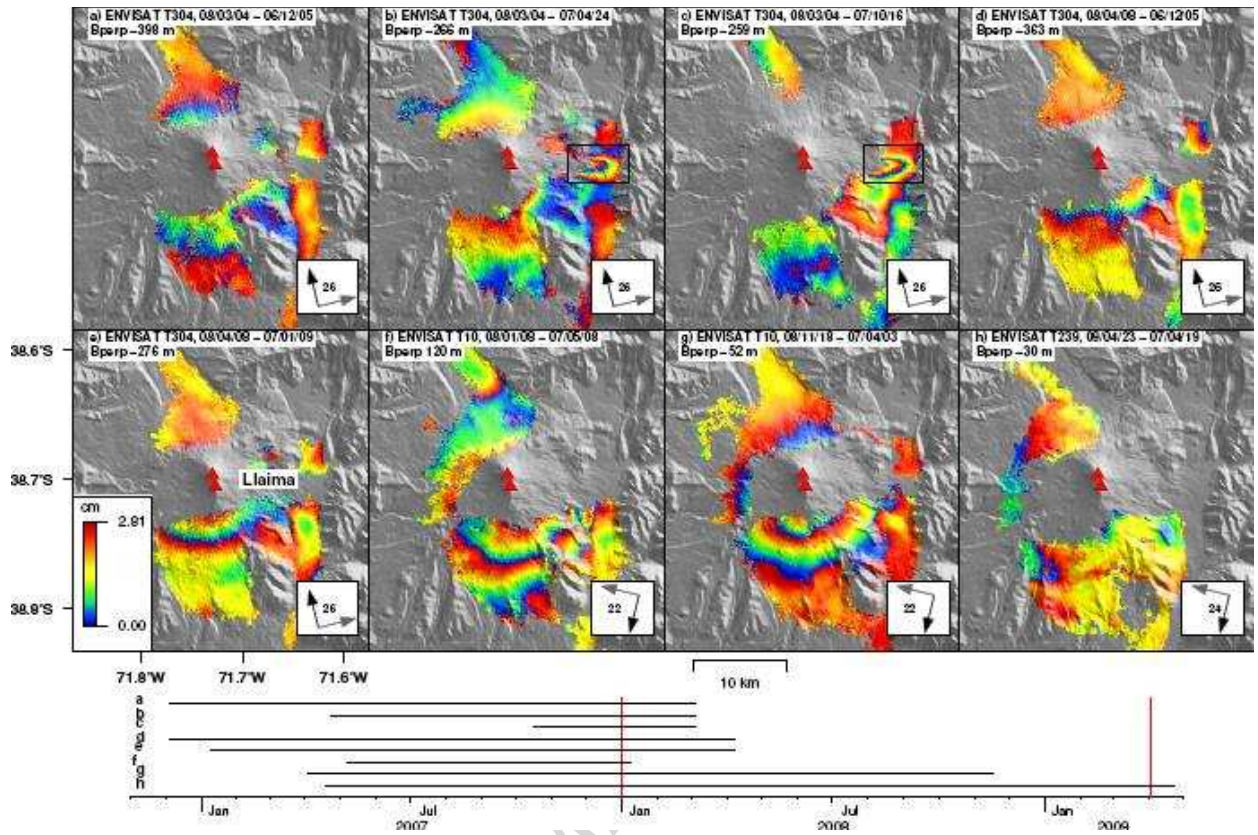


Fig. 4

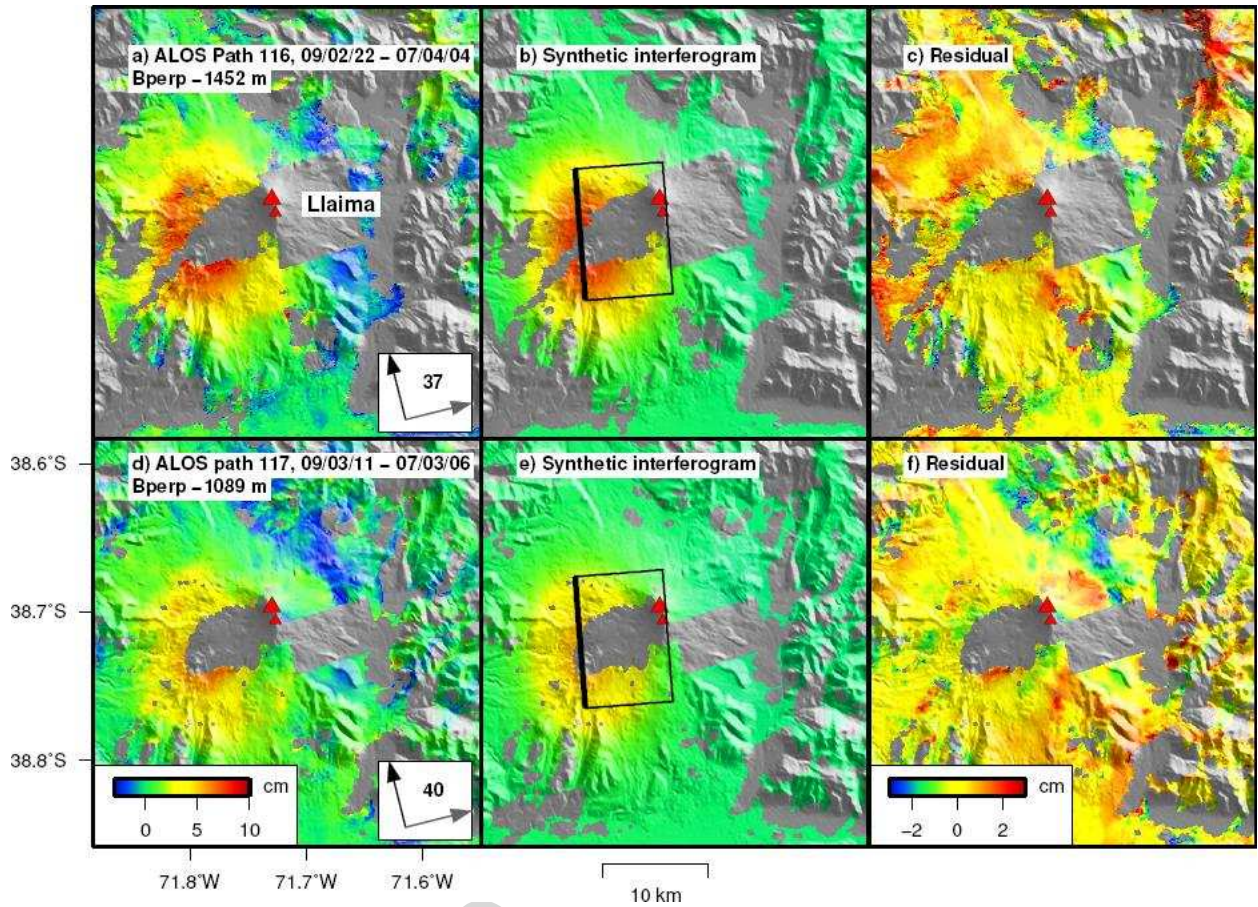


Fig. 5

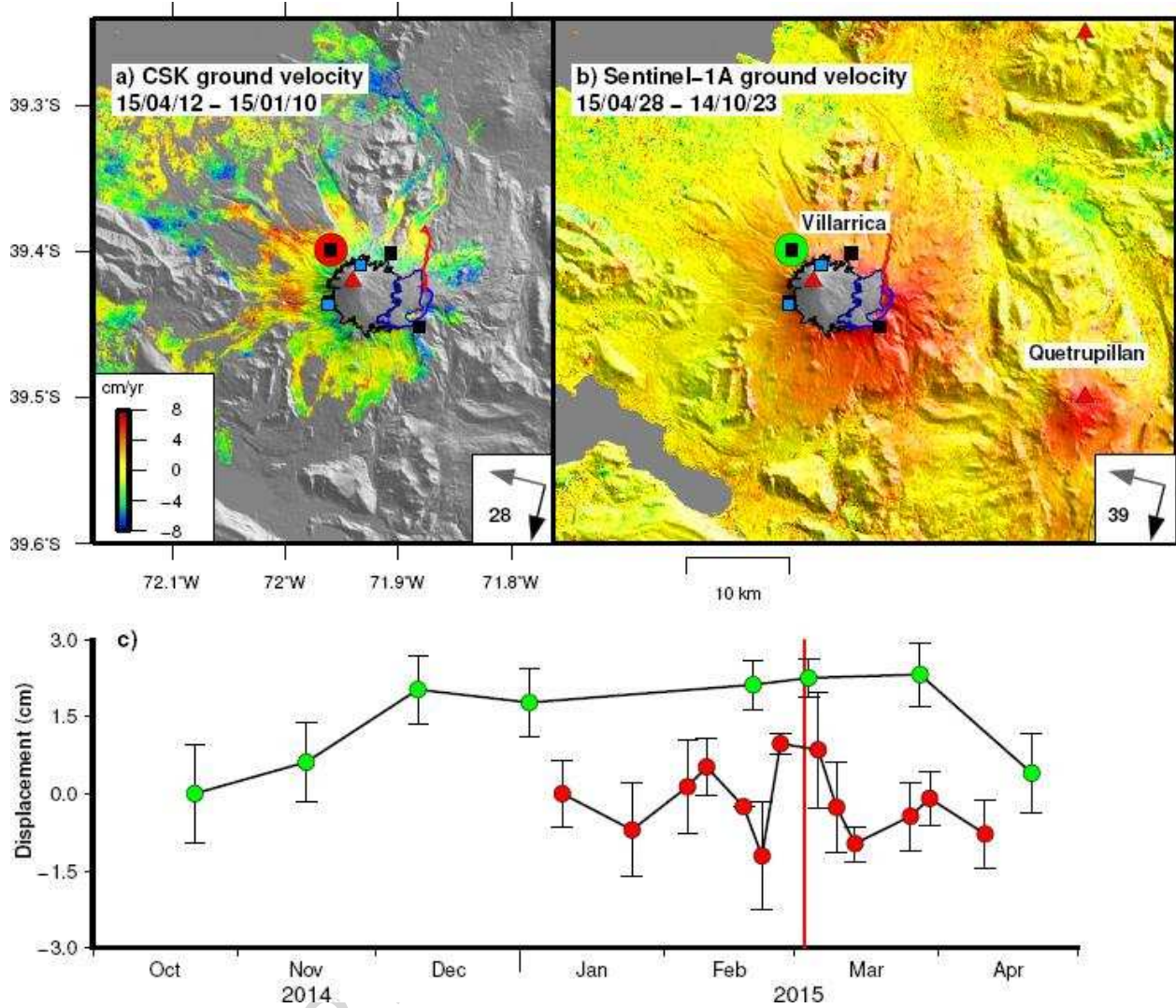


Fig. 6

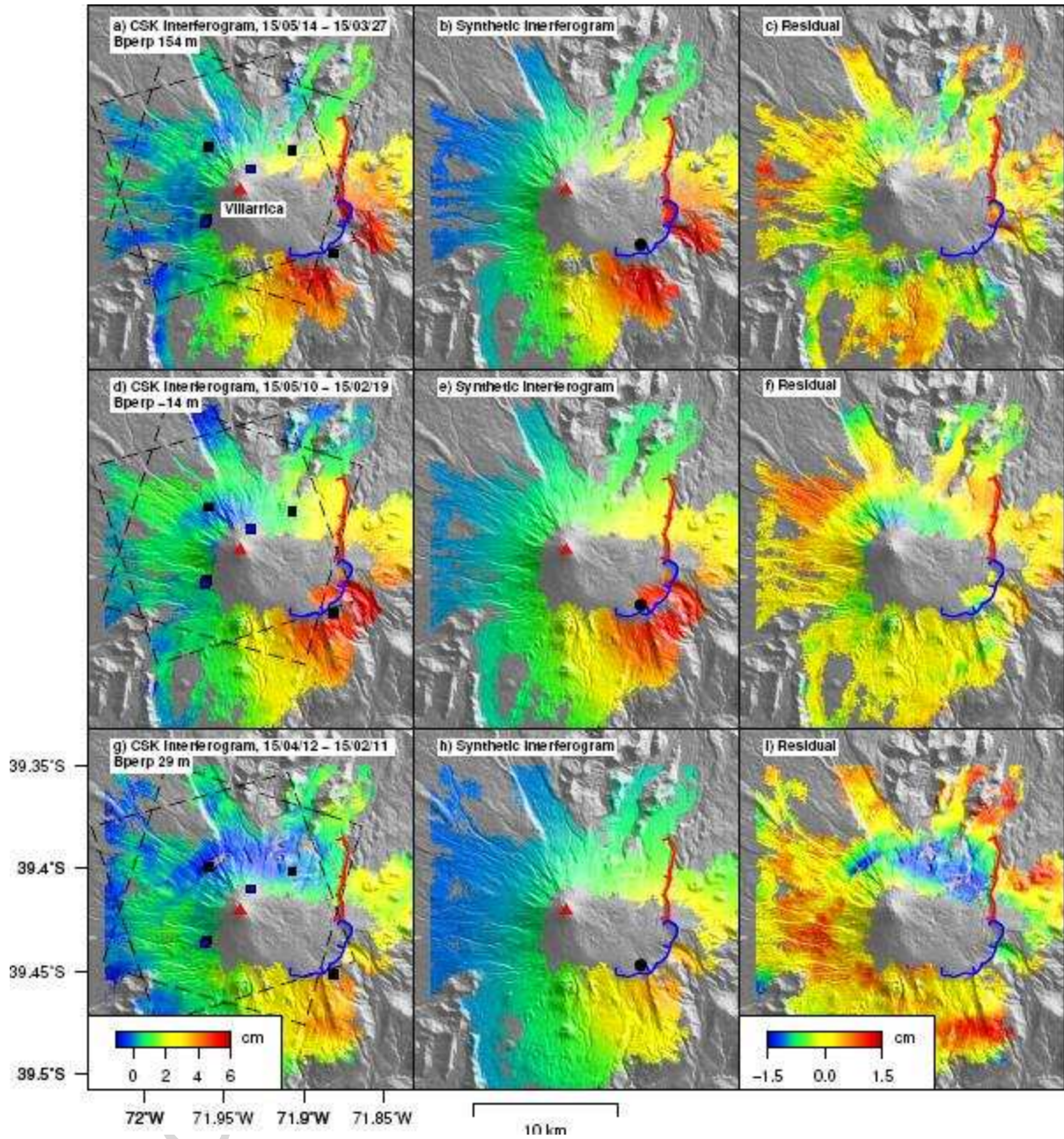


Fig. 7

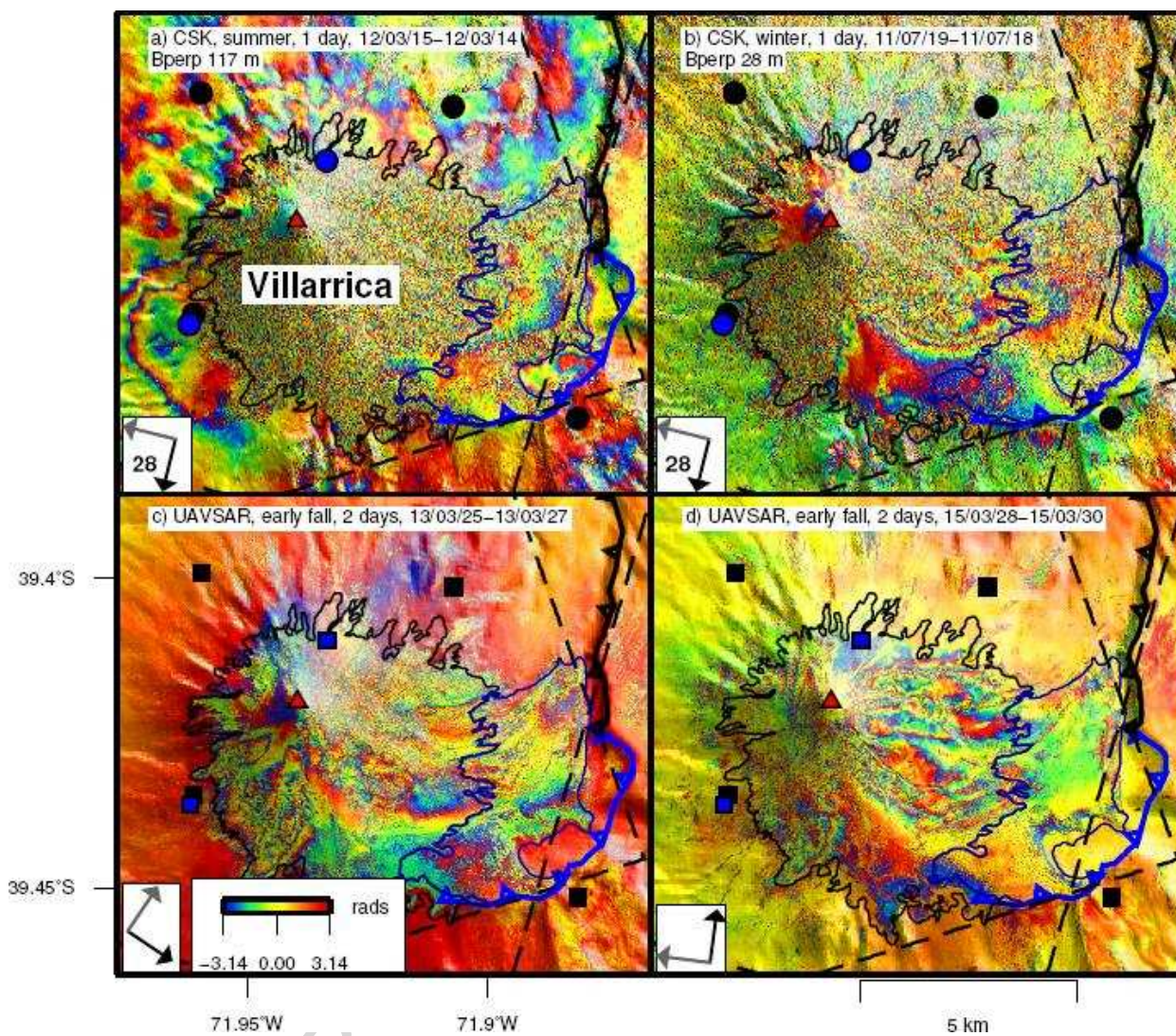


Fig. 9

Highlights

- We present decadal InSAR observations at the three most dangerous volcanoes of the Southern Andes.
- We detect deformation at the three volcanoes at different stages of the eruptive cycle.
- We present the first geodetic source models for the shallow plumbing systems of these volcanoes.
- We do not find evidence that most of the eruptions of these volcanoes were preceded by ground deformation.
- We propose strategies to optimize the use of InSAR as a volcano monitoring tool.